CHEMISTRY
AN ASIAN JOURNAL

DOI: 10.1002/asia.200600067

# Luminescent Molecular Copper(I) Alkynyl Open Cubes: Synthesis, Structural Characterization, Electronic Structure, Photophysics, and Photochemistry

**Chui-Ling Chan, Kai-Leung Cheung, Wai Han Lam, Eddie Chung-Chin Cheng, Nianyong Zhu, Sam Wing-Kin Choi, and Vivian Wing-Wah Yam*[a]**

**Abstract:** A novel class of tetranuclear copper(I) alkynyl complexes with an "open-cube" structure was synthesized. The crystal structure of $[Cu_4\{P(p\text{-}MeC_6H_4)_3\}_4(\mu_3\text{-}\eta^1,\eta^1,\eta^2\text{-}C\equiv C\text{-}p\text{-}MeOC_6H_4)_3]PF_6$ was determined. These complexes were found to display dual emission behavior. Through systematic comparison studies on the electronic absorption and photoluminescence properties of a series of $[Cu_4(PR_3)_4(\mu_3\text{-}\eta^1,\eta^1,\eta^2\text{-}C\equiv CR')_3]^+$ complexes, together with density functional theory (DFT) calculations at the PBE1PBE level on the model complex $[Cu_4(PH_3)_4(\mu_3\text{-}\eta^1,\eta^1,\eta^2\text{-}C\equiv C\text{-}p\text{-}MeOC_6H_4)_3]^+$, the nature of their emission origins was probed. Their photochemical properties were also investigated by oxidative quenching experiments and transient absorption spectroscopy.

**Keywords:** alkyne ligands · copper · density functional calculations · luminescence · photochemistry

## Introduction

The photophysical and photochemical properties of the cubane-type tetranuclear copper(I) complexes have been extensively studied for more than two decades. The luminescence behavior of $[Cu_4X_4L_4]$ (X = halide, L = pyridine) was first reported by Hardt and co-workers.[1] Subsequently, Oelkrug and co-workers reported the presence of two emissive states in the solid state of $[Cu_4I_4py_4]$, with a low-energy (LE) yellow emission band prevailing at room temperature and a high-energy (HE) blue emission band predominating at lower temperature.[2] The emission properties of the complexes $[Cu_4I_4L_4]$ (L = pyridine, morpholine) in benzene were studied by Vogler and co-workers, who proposed that the red luminescence originates from a metal-centered $3d^94s^1$ excited state of copper(I) that has been strongly modified by Cu–Cu interaction.[3] Later, Ford and co-workers extensively investigated the photophysical and photochemical properties of the associated classes of clusters.[3b,4] Ab initio calculations on $[Cu_4I_4py_4]$ supported the assignments that the HE emission is attributed to an iodide-to-pyridine charge transfer (XLCT) origin, whereas the LE emission originates from the cluster-centered (CC) excited state (a mixture of iodide-to-copper charge transfer (XMCT) and metal-centered (MC) [d→s/p] orbital parentage).[4b]

Recently, various extensive series of polynuclear copper(I) and silver(I) alkynyl complexes, such as $[M_3(\widehat{PP})_3(C\equiv CR)_n]^{(3-n)+}$ (M = Cu, Ag; $\widehat{PP}$ = diphosphine; $n$ = 1, 2), $[Cu_3(dppm)_3(C\equiv Ct\text{Bu})Cl]^+$, $[M_3(dppm)_3(C\equiv CC_6H_4\text{-}p\text{-}C\equiv C)M_3(dppm)_3]^{4+}$ (M = Cu, Ag), $[Cu_4(dppm)_4(\mu_4\text{-}\eta^1,\eta^2\text{-}C\equiv C)]^{2+}$, and $[Cu_4(PR_3)_4\{(C\equiv C)_n\text{-}R'\}_4]$ [$n$ = 1 or 2] were isolated[5,6] and their luminescence properties subjected to detailed investigations.[6] These complexes all exhibit intense and long-lived luminescence upon photoexcitation. In view of the interesting structural and photophysical properties of these classes of complexes and as an extension of our previous communication on a tetranuclear copper(I) alkynyl complex, $[Cu_4(PPh_3)_4(\mu_3\text{-}\eta^1,\eta^1,\eta^2\text{-}C\equiv C\text{-}p\text{-}MeOC_6H_4)_3]PF_6$ (**1**), which has an unusual open-cube structure,[7] we report herein the synthesis, characterization, and photophysical and photochemical properties of a series of related tetranuclear copper(I) open cubes, $[Cu_4(PR_3)_4(\mu_3\text{-}\eta^1,\eta^1,\eta^2\text{-}C\equiv CR')_3]PF_6$

[a] Dr. C.-L. Chan, Dr. K.-L. Cheung, Dr. W. H. Lam, Dr. E. C.-C. Cheng, Dr. N. Zhu, Dr. S. W.-K. Choi, Prof. Dr. V. W.-W. Yam
Centre for Carbon-Rich Molecular and Nano-Scale Metal-Based Materials Research and
Department of Chemistry
University of Hong Kong
Pokfulam Road, Hong Kong SAR (China)
Fax: (+852) 2857-1586
E-mail: wwyam@hku.hk

Supporting information for this article is available on the WWW under http://www.chemasianj.org or from the author.

  

(R = Ph, R′ = *p*-$EtOC_6H_4$ (**2**), *p*-*n*$BuOC_6H_4$ (**3**), *p*-*n*Hex-$OC_6H_4$ (**4**), *p*-*n*$HeptOC_6H_4$ (**5**), *p*-$MeC_6H_4$ (**6**), *p*-*n*$BuC_6H_4$ (**7**), *p*-*n*$HexC_6H_4$ (**8**), *p*-*n*$HeptC_6H_4$ (**9**), *p*-*n*$OctC_6H_4$ (**10**), *p*-$PhC_6H_4$ (**11**), *p*-$ClC_6H_4$ (**12**), $C_4H_3S$ (**13**); R′ = *p*-$MeOC_6H_4$, R = *p*-$MeC_6H_4$ (**14**), *p*-$CF_3C_6H_4$ (**15**)) (Scheme 1). It is hoped that through a systematic and judicious choice of alkynyl ligands and ancillary phosphine ligands, together with DFT calculations, further insight into the role played by these ligands in the spectroscopic origin of this class of complexes could be provided. The excited-state properties were also investigated by oxidative quenching experiments and transient absorption spectroscopy.

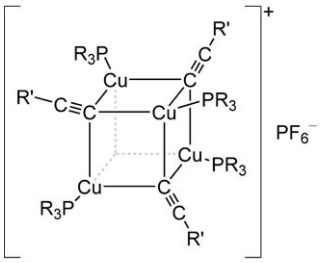


| | | |
|---|---|---|
| R = Ph, R′ = *p*-$MeOC_6H_4$ | **1** |
| R = Ph, R′ = *p*-$EtOC_6H_4$ | **2** |
| R = Ph, R′ = *p*-*n*$BuOC_6H_4$ | **3** |
| R = Ph, R′ = *p*-*n*$HexOC_6H_4$ | **4** |
| R = Ph, R′ = *p*-*n*$HeptOC_6H_4$ | **5** |
| R = Ph, R′ = *p*-$MeC_6H_4$ | **6** |
| R = Ph, R′ = *p*-*n*$BuC_6H_4$ | **7** |
| R = Ph, R′ = *p*-*n*$HexC_6H_4$ | **8** |
| R = Ph, R′ = *p*-*n*$HeptC_6H_4$ | **9** |
| R = Ph, R′ = *p*-*n*$OctC_6H_4$ | **10** |
| R = Ph, R′ = *p*-$PhC_6H_4$ | **11** |
| R = Ph, R′ = *p*-$ClC_6H_4$ | **12** |
| R = Ph, R′ = $C_4H_3S$ | **13** |
| R = *p*-$MeC_6H_4$, R′ = *p*-$MeOC_6H_4$ | **14** |
| R = *p*-$CF_3C_6H_4$, R′ = *p*-$MeOC_6H_4$ | **15** |

Scheme 1. Tetranuclear copper(I) alkynyl "open-cube" complexes.

## Results and Discussion

### Synthesis and Characterization

Reaction of $[Cu(MeCN)_4]PF_6$ with triaryl phosphine ($PR_3$) and the appropriate gold(I) alkynyl polymer, $[Au(C{\equiv}CR')]_\infty$ in dichloromethane under a stream of dry nitrogen afforded the tetranuclear copper(I) alkynyl complexes, $[Cu_4(PR_3)_4(\mu_3\text{-}\eta^1,\eta^1,\eta^2\text{-}C{\equiv}CR')_3]PF_6$. All the newly synthesized copper(I) complexes appear as pale yellow crystals, which are both air- and moisture-stable in the solid state. However, they are stable only for a few weeks in the absence of light in solution in dichloromethane and acetone, with the exception of the 4-chlorophenylalkynyl counterpart which is only stable for 3–4 days. Moreover, in the course of the preparation of these tetranuclear copper(I) alkynyl complexes, $[Au(PPh_3)_2]^+$ was isolated as a by-product.

All the newly synthesized copper(I) complexes gave satisfactory elemental analyses, and were characterized by $^1H$ NMR spectroscopy, IR spectroscopy, and positive-ion FAB and ESI mass spectrometry.

The IR spectra of all the copper(I) alkynyl complexes revealed a strong band at $\approx 840\ cm^{-1}$, characteristic of $PF_6^-$ absorption. The C≡C stretching modes were, however, too weak to be observed.

The positive-ion FAB and ESI mass spectra of all the copper(I) alkynyl complexes showed similar patterns. In most of the mass spectra, peaks corresponding to the respective $\{[Cu_4(PR_3)_4(C{\equiv}CR')_3]\}^+$ ions appeared. An exception was found for **15** for which the mass peak of the parent cation ($[M-PF_6]^+$) was not observed, which may be attributed to the relatively more labile nature of the trifluoromethylphenyl-substituted phosphine as a result of its poorer electron-donating properties. Instead, peaks corresponding to the $[Cu_3\{P(p\text{-}CF_3C_6H_4)_3\}_3(C{\equiv}C\text{-}p\text{-}MeOC_6H_4)_3]^+$ and $[Cu_4\{P(p\text{-}CF_3C_6H_4)_3\}_2(C{\equiv}C\text{-}p\text{-}MeOC_6H_4)_3]^+$ ion clusters were observed in the FAB and ESI mass spectra, respectively.

In addition, the X-ray crystal structures of **1** and **14** were determined. The X-ray crystal structure of **1** has already been communicated.[7] Single crystals of **14** were obtained by slow vapor diffusion of diethyl ether into a concentrated solution of the complex in dichloromethane. Figure 1 depicts the perspective view of the complex cation of **14** with its atomic numbering scheme; the crystal and structure-determination data as well as selected bond distances and angles are summarized in Table 1 and Table 2, respectively. Both crystal structures revealed that the complex cation adopts an open-cube structure, that is, a cubane structure similar to

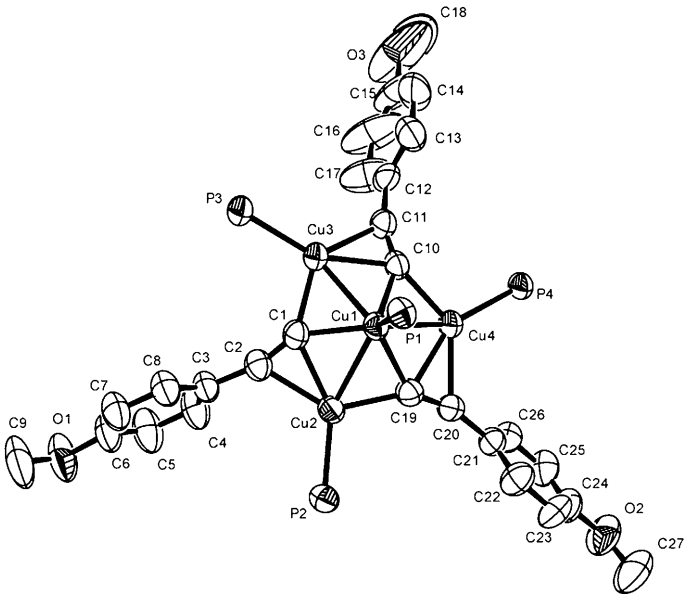


Figure 1. Perspective drawing of the complex cation of **14** with atomic numbering scheme. Thermal ellipsoids are shown at the 30% probability level. Hydrogen atoms and the tolyl groups have been omitted for clarity.

**Abstract in Chinese:**

本文報導了一系列具有開立方體式分子結構的新類四核銅(I)炔基配合物的合成，其中$[Cu_4\{P(C_6H_4Me\text{-}p)_3\}_4(\mu_3\text{-}\eta^1,\eta^1,\eta^2\text{-}C{\equiv}CC_6H_4OMe\text{-}p)_3]PF_6$的晶體結構亦被確定。我們發現這些配合物具有雙性發光行爲，並通過一系列$[Cu_4(PR_3)_4(\mu_3\text{-}\eta^1,\eta^1,\eta^2\text{-}C{\equiv}CR')_3]^+$的電子吸收和光致發光性質的系統性相比研究，以及對一模型配合物$[Cu_4(PH_3)_4(\mu_3\text{-}\eta^1,\eta^1,\eta^2\text{-}C{\equiv}CC_6H_4OMe\text{-}p)_3]^+$進行 PBE1PBE 層級的密度泛函理論(DFT)計算來闡明它們的發光源由。此外，我們通過氧化淬滅實驗和瞬態吸收光譜學來深入探索它們的光化學性質。

  

Table 1. Crystal and structure determination data for **14**.

| | |
|---|---|
| Formula | $C_{111}H_{105}Cu_4F_6O_3P_5 \cdot {}^1/_2H_2O$ |
| *FW* | 2018.97 |
| *T* [K] | 301(2) |
| *a* [Å] | 15.720(3) |
| *b* [Å] | 29.485(6) |
| *c* [Å] | 22.687(5) |
| *β* [deg] | 98.26(3) |
| *V* [Å$^3$] | 10406(4) |
| Crystal system | monoclinic |
| Space group | $P2_1/n$ (No. 14) |
| *Z* | 4 |
| *F*(000) | 4180 |
| $\rho_{calcd}$ [g cm$^{-3}$] | 1.289 |
| Crystal color/shape | pale yellow crystal |
| Crystal dimensions [mm] | 0.40×0.40×0.15 |
| *λ* [Å] (graphite monochromated, $Mo_{K\alpha}$) | 0.71073 |
| *M* [cm$^{-1}$] | 9.43 |
| *Θ* range for data collection | 1.48 to 25.50° |
| Index ranges | *h*: −18 to 18; *k*: −35 to 35, *l*: −27 to 26 |
| Data collection mode | 2° oscillation (101 images), 120-mm distance, 300-s exposure |
| No. of data collected | 48264 |
| No. of unique data | 15613 |
| $R_{int}$ | 0.0508 |
| No. of data used in refinement [*n*] | 15613 |
| No. of parameter refined [*p*] | 1163 |
| $R(F_o)$[a] | 0.0547 |
| $R_w(F_o)$[b] | 0.1584 |
| *S*[c] | 0.942 |
| Maximum shift $[(\Delta/\sigma)_{max}]$ | 0.003 (av. 0.001) |
| Residual extrema in final difference map [e Å$^{-3}$] | 1.782, −0.736 |

[a] $R_{int}=\Sigma||F_o|-|F_c||/\Sigma|F_o|$. [b] $R_w=\{\Sigma[w(F_o^2-F_c^2)^2]/\Sigma[w(F_o^2)^2]\}^{1/2}$ with $w=1/[\sigma^2(F_o^2)+(aP)^2+bP]$, where $P=[2F_c^2+\mathrm{Max}(F_o^2,0)]/3$. [c] $S=\{\Sigma[w(F_o^2-F_c^2)^2]/(n-p)\}^{1/2}$.

Table 2. Selected bond lengths [Å] and bond angles [deg] for **14** with estimated standard deviations in parentheses.

| Bond lengths (Å) | | | |
|---|---|---|---|
| Cu1−C1 | 2.063(6) | Cu3−C1 | 2.054(5) |
| Cu1−C19 | 2.099(5) | Cu3−C10 | 2.105(5) |
| Cu1−C10 | 2.109(5) | Cu3−C11 | 2.151(6) |
| Cu1−P1 | 2.2544(16) | Cu3−P3 | 2.2358(16) |
| Cu1−Cu4 | 2.4607(9) | Cu4−C10 | 2.041(5) |
| Cu1−Cu3 | 2.4660(9) | Cu4−C19 | 2.109(5) |
| Cu1−Cu2 | 2.4791(10) | Cu4−C20 | 2.128(5) |
| Cu2−C19 | 2.026(6) | Cu4−P4 | 2.2281(15) |
| Cu2−C1 | 2.089(5) | C1−C2 | 1.236(7) |
| Cu2−C2 | 2.139(6) | C10−C11 | 1.231(7) |
| Cu2−P2 | 2.2333(15) | C19−C20 | 1.238(7) |
| **Bond angles (deg)** | | | |
| C2−C1−Cu3 | 137.8(4) | Cu3−C10−Cu1 | 71.65(16) |
| C2−C1−Cu1 | 147.6(4) | Cu4−C10−Cu1 | 72.71(18) |
| Cu3−C1−Cu1 | 73.58(19) | C10−C11−C12 | 159.6(5) |
| C2−C1−Cu2 | 75.2(3) | C10−C11−Cu3 | 71.1(3) |
| Cu3−C1−Cu2 | 137.6(3) | C20−C19−Cu2 | 143.7(4) |
| Cu1−C1−Cu2 | 73.32(17) | C20−C19−Cu1 | 142.0(4) |
| C1−C2−C3 | 163.7(6) | Cu2−C19−Cu1 | 73.86(19) |
| C1−C2−Cu2 | 70.8(4) | C20−C19−Cu4 | 73.9(3) |
| C11−C10−Cu4 | 140.2(4) | Cu2−C19−Cu4 | 133.3(3) |
| C11−C10−Cu3 | 75.3(4) | Cu1−C19−Cu4 | 71.59(15) |
| Cu4−C10−Cu3 | 138.3(3) | C19−C20−C21 | 161.9(5) |
| C11−C10−Cu1 | 146.3(4) | C19−C20−Cu4 | 72.2(3) |

that of $[Cu_4X_4L_4]$ (X = halogen, L = N, P as donor; X = alkynyl, L = P donor)[6a–c,8] but with a vertex missing. Such an open-cube structure, which is known to exist in a number of metal clusters such as those of iron and molybdenum, is rarely found in copper(I).[9] To the best of our knowledge, in addition to the previously communicated complex **1**,[7] the only known examples reported are those found in $[Cu_4Cl(PPh_2)_3(PPh_2nPr)_3]$[10a] and $[Cu_4Cl(PPh_2)_3(PMe_3)_4]$,[10b] with no precedents in alkynyl complexes. The complex cation of **14** consists of a puckered $Cu_3C_3$ six-membered ring, which is bridged by a central Cu1 and three alkynyl groups in $\mu_3$-bridging modes. The Cu1−Cu2, Cu1−Cu3, and Cu1−Cu4 distances of 2.4607(9)–2.4791(10) Å are found to be much shorter than the Cu···Cu distances found within the $Cu_3C_3$ ring (3.80–3.88 Å). This suggests the electron-deficient nature of the three-center-two-electron Cu1−C−Cu bonding. The slightly longer Cu···Cu distances in **14** than those in **1** (2.446(2)–2.467(2) Å) are in line with the higher electron richness of the ancillary phosphines. The acute Cu1−C−Cu angles of 71.65(16)–72.71(18)° further indicate the electron deficiency of these three-center-two-electron bonds. The copper atoms in the $Cu_3C_3$ ring, on the other hand, are relatively less electron-deficient owing to possible π-electron donation by side-on coordination of the C≡CR′ ligand to each of the copper centers in the ring. Interestingly, the structure of **14** differs from that of the related organocopper(I) cluster, $[Cu_4\{P(p\text{-}MeC_6H_4)_3\}_4(\mu_3\text{-}\eta^1\text{-}C{\equiv}CPh)_4]$,[5b] which has a distorted close-cubane geometry. The Cu···Cu distances found in **14** [2.4607(9)–2.4791(10) Å] are comparable to those found in $[Cu_4Cl(PPh_2)_3(PMe_3)_4]$ [2.4836(8)–2.5345(8) Å],[10b] but much shorter than those found in close-cubane-type complexes such as $[Cu(PPh_3)X]_4$ (X = Cl, Br, I) [2.874(5)–3.541(2) Å][8b,d] and $[Cu_4(PAr_3)_4(\mu_3\text{-}\eta^1\text{-}C{\equiv}CPh)_4]$ (Ar = Ph, p-$FC_6H_4$F, p-$MeC_6H_4$) [2.5092(5)–2.6635(8) Å].[5b] Such short Cu···Cu distances are not uncommon in organocopper systems, particularly those that are electron deficient, and may not necessarily indicate a metal–metal interaction.[11] The presence of side-on π bonding between the C≡C groups and the copper(I) centers gives rise to the bent C≡C−C geometry (C1−C2−C3 163.7(6)°, C10−C11−C12 159.6(5)°, C19−C20−C21 161.9(5)°).

In view of the electron-deficient nature and the interesting open-cube structures of **1**–**15**, attempts to utilize these complexes as precursors to synthesize close-cubane-type complexes through the ligation of an additional anionic ligand, such as an alkynyl or a thiolate, to the unoccupied vertex were made but have been unsuccessful so far.

### Electronic Absorption Spectroscopy

All the copper(I) alkynyl complexes are soluble in dichloromethane and give pale-yellow solutions. The electronic absorption spectral data are collected in Table 3. The electronic absorption spectra of all the copper(I) alkynyl complexes

  

at 298 K are characterized by a high-energy absorption band at ≈252–270 nm and a band at ≈328–340 nm with a tail extending to 400 nm. Additional shoulders are observed for complexes **5–11** and **15** at ≈268–282 nm, with vibrational progressional spacings of ≈1100–1300 $cm^{-1}$, which are typical of the skeletal vibrational modes of the aromatic rings. The high-energy absorption band at ≈252–260 nm is assigned as the intraligand transition of the phosphine ligands as the free ligands also absorb strongly in this region. The only absorption spectral feature unique to these open-cube complexes is the long-wavelength absorption at ≈328–340 nm that tails to ≈400 nm. These low-energy absorptions may be due to metal-to-ligand charge transfer (MLCT) [3d(Cu)→π*(C≡CAr)] (Ar = aromatic ring), metal-perturbed intraligand (IL) [π→π*(C≡CAr)], ligand-to-metal charge transfer (LMCT) [π(C≡CAr)→4s/p(Cu)], and metal-centered (MC) [3d→4s/p(Cu)] transitions. However, since the absorption patterns are rather broad and featureless, the absorption spectra provide no convincing evidence about the nature of the transitions involved, and no further attempts were made to assign these LE bands unambiguously.

Table 3. Photophysical and electrochemical data for the tetranuclear copper(I) alkynyl open-cube complexes.

| Complex | $\lambda_{max}$ [nm] ($\varepsilon_{max}$ [$dm^3 mol^{-1} cm^{-1}$])[a] | Emission | |
|---|---|---|---|
| | | Medium ($T$ [K]) | $\lambda_{em}$ [nm] ($\tau_0$ [μs]) |
| **1**[b] | 252 sh (88550), 330 (48925) | solid (298) | 445, 630 (20.7) |
| | | solid (77) | 445 |
| | | $CH_2Cl_2$ (298) | 675 (2.7) |
| **2** | 256 sh (132190), 336 (26670) | solid (298) | 455, 627 (7.5) |
| | | solid (77) | 448, 465 |
| | | $CH_2Cl_2$ (298) | 668 (2.4) |
| **3** | 258 sh (99310), 334 (43500) | solid (298) | 453, 485 (2.6) |
| | | solid (77) | 449, 470 |
| | | $CH_2Cl_2$ (298) | 670 (1.7) |
| **4** | 260 sh (78260), 332 (45750) | solid (298) | 453, 623 (5.7) |
| | | solid (77) | 446, 482 |
| | | $CH_2Cl_2$ (298) | 670 (2.5) |
| **5** | 258 sh (99370), 278 (49410), 332 (39610) | solid (298) | 455 (8.76), 630 (3.22) |
| | | solid (77) | 446, 483 |
| | | $CH_2Cl_2$ (298) | 670 (2.84) |
| **6** | 254 sh (67640), 268 sh (52680), 276 sh (50890), 330 (36920) | solid (298) | 458 (1.28), 633 (3.74) |
| | | solid (77) | 453, 487, 665 |
| | | $CH_2Cl_2$ (298) | 666 (2.84) |
| **7** | 254 sh (87450), 274 (40150), 334 (29790) | solid (298) | 449, 480 (7.6) |
| | | solid (77) | 446, 484 |
| | | $CH_2Cl_2$ (298) | 665 (3.7) |
| **8** | 256 sh (96540), 282 (48870), 328 (59890) | solid (298) | 456, 626 (4.3) |
| | | solid (77) | 448, 485 |
| | | $CH_2Cl_2$ (298) | 668 (3.9) |
| **9** | 258 sh (75370), 281 (45280), 328 (37480) | solid (298) | 455, 634 (5.7) |
| | | solid (77) | 450, 500 |
| | | $CH_2Cl_2$ (298) | 670 (4.0) |
| **10** | 258 sh (85290), 278 (69350), 326 (41590) | solid (298) | 450, 482 (9.5) |
| | | solid (77) | 448, 480 |
| | | $CH_2Cl_2$ (298) | 664 (3.6) |
| **11** | 252 sh (66360), 276 sh (59070), 286 sh (57270), 340 (62620) | solid (298) | 509, 541 (7.83) |
| | | solid (77) | 500, 540 |
| | | $CH_2Cl_2$ (298) | 675 (3.56) |
| **12** | 254 sh (59510), 334 (44430) | solid (298) | 461, 490 (30.0) |
| | | solid (77) | 456, 492 |
| | | $CH_2Cl_2$ (298) | 666 (3.32) |
| **13** | 270 sh (39060), 278 sh (33210), 298 sh (25270), 314 (16930), 342 (9960) | solid (298) | 549 (11.7), 665 (5.7) |
| | | solid (77) | 546, 660 |
| | | $CH_2Cl_2$ (298) | 700 (2.0) |
| **14** | 258 sh (93180), 332 (15090) | solid (298) | 466, 483 (8.7) |
| | | solid (77) | 454, 495 |
| | | $CH_2Cl_2$ (298) | 670 (3.1) |
| **15** | 260 sh (62370), 278 (49510), 328 (21570) | solid (298) | 444 (5.6), 631 (0.7) |
| | | solid (77) | 440, 479 |
| | | $CH_2Cl_2$ (298) | 680 (2.4) |

[a] Absorption in $CH_2Cl_2$ at 298 K. [b] From reference [7].

### Steady-State Emission Spectroscopy

Excitation of solid or fluid solutions of all the open-cube copper(I) alkynyl complexes at $\lambda > 350$ nm produced long-lived, intense luminescence. Their photophysical data are tabulated in Table 3. The solid state emission spectra of representative complexes **4** and **10** at 298 K and 77 K are displayed in Figure 2 and Figure 3, respectively. The solid-state emission spectra of all the open-cube complexes show a high-energy emission band at ≈443–541 nm. The intense high-energy bands are structured at 77 K with vibrational progressional spacings of ≈1200–1640 $cm^{-1}$, typical of the $\nu$(C≡C) stretches in the ground state.

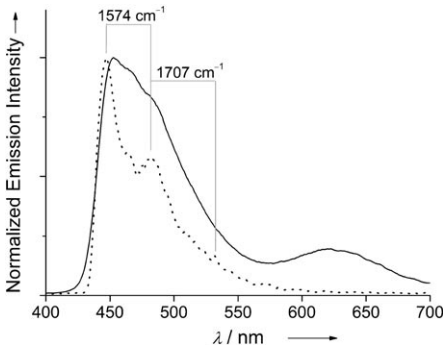


Figure 2. Solid-state emission spectra of **4** at 298 K (——) and 77 K (·····).

  

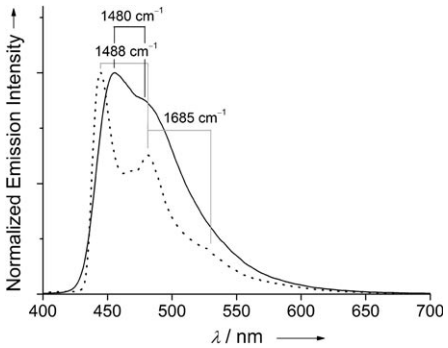


Figure 3. Solid-state emission spectrum of **10** at 298 K (——) and 77 K (·····).

For some of the open-cube complexes such as **1**, **2**, **4**, **5**, **6**, **8**, **9**, **13**, and **15**, an additional low-energy emission band at ≈623–665 nm was observed in the solid-state emission spectra. These two emissions were believed to have different origins as their excitation spectra were substantially different despite some overlap in the spectra. For example, complex **6** exhibits excitation band maxima at ≈400 and ≈350 nm for the green and orange emissions, respectively. The results indicate that the Stokes shift for the low-energy emission is considerably larger than that for the high-energy emission, as the excitation band corresponding to the low-energy emission is at a higher energy than that of the high-energy emission. A similar observation was also made in the $[Cu_4I_4L_4]$ system.[4]

In contrast, all the open-cube complexes exhibit only the orange phosphorescence in solution in dichloromethane at ambient temperature. The emission spectrum of **10** in dichloromethane is depicted in Figure 4 as a representative example. All the spectra show a single structureless band centered at ≈665–700 nm. The consistent red shift in the emission energy of such orange phosphorescence in fluid solutions of **1**, **2**, **4**, **5**, **6**, **8**, **9**, **13**, and **15** compared to that in solid samples of the respective complexes is indicative of the presence of rigidochromism. The lifetime of the excited state in the microsecond range suggests that the emission is most likely associated with a spin-forbidden transition from a triplet state. The observation of a single emission band and the close analogies of the photophysical properties of

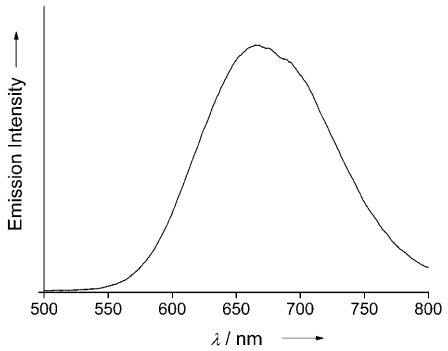


Figure 4. Emission spectrum of **10** in degassed dichloromethane at 298 K.

these complexes in solution further confirm that the complexes maintain their molecular integrity and remain intact in solution.

In general, the high-energy emission energies follow an order with R′ = alkoxyphenyl ≥ alkylphenyl > chlorophenyl > biphenyl > thienyl. This trend is in agreement with the energy gap between the π and π* orbitals of the substituted ethynyl ligands. Attachment of an electron-donating group such as alkyl and alkoxy to the phenylethynyl ligand would give rise to a larger π–π* energy gap, whereas an extended π conjugation in biphenylethynyl would lower the π–π* energy gap. The thienyl group is expected to have a smaller π-π* energy gap than the aryl moieties owing to the weaker π-bonding interaction of the C–S bond relative to the C–C bond, resulting from the poor π overlap between the more diffuse S 3p and C 2p orbitals. Therefore, it is possible that this high-energy emission originates from the intraligand π–π* state of the alkynyl ligand. Nevertheless, one could not eliminate the possibility of an emission origin that has a substantial MLCT [Cu→π*(RC≡C)] character.

An involvement of copper(I) character in the LUMO could be inferred from the emission energy trend of the low-energy orange phosphorescence in dichloromethane: **14** ≥ **1** > **15**, in which the more-electron-rich phosphine ligands would render the copper(I) centers more electon-rich and hence make the associated metal-centered acceptor orbitals higher-lying in energy. Furthermore, for the complexes with the ancillary $PPh_3$ ligands, the energy of the orange emission in $CH_2Cl_2$ at 298 K follows the order R′ = chlorophenyl ≥ alkylphenyl > alkoxyphenyl > biphenyl > thienyl, in line with an assignment of an emissive state derived from a LMCT [π(C≡CAr)→4s/p(Cu)] origin. The large Stokes shift of this low-energy emission implies a significant distortion of the associated excited state relative to the ground state. It could be possible that such an excited state involves the population of electron density in the bonding orbital with respect to the Cu···Cu interactions within the $Cu_4$ cluster core, causing a significant structural distortion of the $Cu_4$ core. With reference to the spectroscopic works by the groups of Vogler, Ford, and Yam on the related polynuclear copper(I) systems,[3–5] it is likely that the low-energy emission originates from the LMCT [RC≡C·→$Cu_4$] excited states, mixed with the copper(I)-centered d-s/d-p characters that have been modified by Cu···Cu interaction owing to configurational mixing of the filled orbitals of 3d parentage with the appropriate empty orbitals derived from the higher energy 4 s and 4p atomic orbitals of the tetrameric copper unit (d→s/d→p), or alternatively, the metal cluster-centered excited states. A detailed assignment of the spectroscopic origins will be discussed in light of the studies on the electronic structures by DFT calculations.

## Electronic Structure Calculations

In view of the interesting solid-state dual luminescence behavior found in some of the complexes and the large Stokes shift observed for the low-energy band at ≈623–665 nm,

  

DFT calculations at the PBE1PBE level were employed to study the electronic structures of the ground and excited states of this class of tetranuclear copper(I) alkynyl open-cube complexes, and to provide some insight into the extent of the distortion in the excited states relative to that of the ground state. To decrease the time and costs of computation, a model complex $[Cu_4(PH_3)_4(\mu^3\text{-}\eta^1,\eta^1,\eta^2\text{-}C\equiv C\text{-}p\text{-}MeOC_6H_4)_3]^+$ (**1a**) was employed to mimic **1**, in which all the phenyl rings on the phosphine ligands were replaced by hydrogen atoms. Geometry optimizations of **1a** were performed both in the presence and absence of a $C_3$-symmetry constraint (taking the $C_3$ axis to be along the Cu1–P1 bond), from which both cases led to the same resultant geometry and energy. Thus only the electronic structure of **1a** with the $C_3$ symmetry will be discussed. Figure 5 depicts the calculated geometry for **1a**, where the open-cube structure is reproduced. Selected calculated structural parameters for **1a** and comparison with the crystal structural data of **1** are also shown in Figure 5. The optimized structural parameters are in excellent agreement with the experimental values, indicating that the model and the level of theory that we applied are appropriate and reliable. On the basis of the experimental and calculated structural parameters, a simple bonding picture for the tetranuclear copper open-cube cluster is suggested (Scheme 2). The central copper atom exhibits distorted tetrahedral geometry and is coordinated by a phosphine ligand as well as three three-center-two-electron bonds among the $Cu_{center}$, $C_\alpha$, and $Cu_{peripheral}$ atoms. On the other hand, the three peripheral copper atoms have a distorted trigonal-planar arrangement, with each of them coordinated by a phosphine ligand and a three-center-two-electron bond originating from side-on $\pi$ bonding of the C≡C unit.

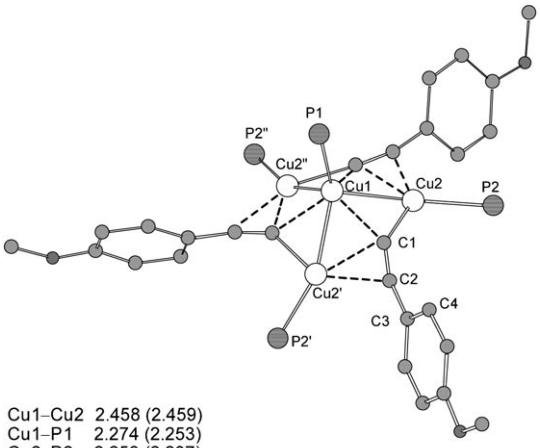


| | |
|---|---|
| Cu1–Cu2 | 2.458 (2.459) |
| Cu1–P1 | 2.274 (2.253) |
| Cu2–P2 | 2.258 (2.237) |
| C1–Cu2 | 2.012 (2.022) |
| C1–Cu1 | 2.120 (2.119) |
| C1–Cu2" | 2.115 (2.118) |
| C2–Cu2" | 2.156 (2.120) |
| C1–C2 | 1.256 (1.240) |
| C2–C3 | 1.434 (1.450) |

| | |
|---|---|
| P1–Cu1–Cu2 | 118.8 (116.0) |
| C3–C2–C1 | 165.5 (163.8) |
| C4–C3–C2–C1 | 52.1 (58.2) |

Figure 5. Selected structural parameters for **1a** ($C_3$ symmetry) optimized at the PBE1PBE level of theory, together with the experimental structural parameters of **1** in parentheses. The distances and angles are in Å and degrees, respectively. Hydrogen atoms are omitted for simplicity.

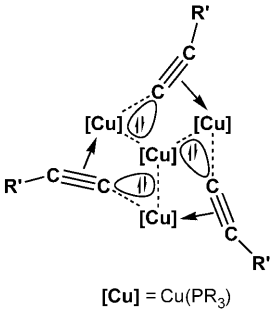


Scheme 2. Simplified bonding picture for **1**–**15**.

The selected frontier orbitals, together with their percentage contributions estimated from the Mulliken population analysis, are shown in Figure 6. The three highest occupied and three lowest unoccupied orbitals were found to be localized mainly on the C≡C-*p*-$MeOC_6H_4$ units, with small to moderate contributions (≈10–33%) from the copper orbitals. The occupied orbitals can be described as a linear combination of the three highest-occupied $\pi$ orbitals of the C≡C-*p*-$MeOC_6H_4$ units, forming the high-energy de-

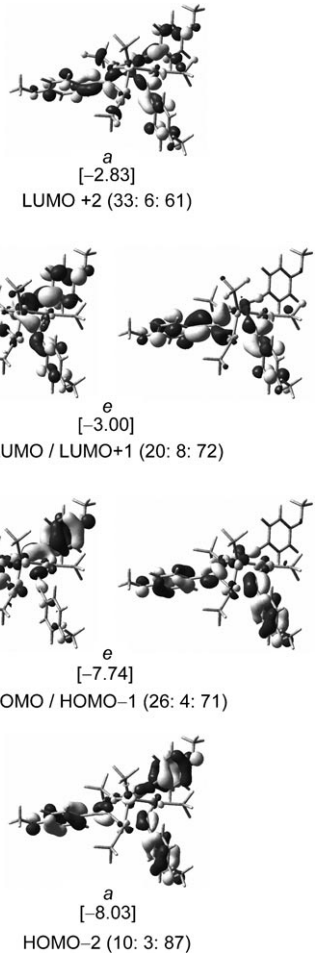


Figure 6. Spatial plots (isovalue = 0.03) of the three HOMOs and three LUMOs for **1a** at the ground-state optimized geometry, with their orbital energy (eV) in square brackets. The percentage contributions are expressed in terms of the four copper atoms (Cu), four phosphine ligands ($PH_3$), and three C≡C-*p*-$MeOC_6H_4$ ligands in parentheses (Cu: $PH_3$: C≡C-*p*-$MeOC_6H_4$).

  

CHEMISTRY
AN ASIAN JOURNAL

generate orbitals of *e* symmetry and a low-energy orbital of *a* symmetry, whereas the unoccupied orbitals are the linear combinations of the three π* orbitals of the C≡C-*p*-$MeOC_6H_4$ units, forming the low-energy degenerate orbitals of *e* symmetry and a high-energy orbital of *a* symmetry. On the basis of the frontier orbitals of **1a**, the lowest energy absorptions of $[Cu_4(PR_3)_4(\mu^3\text{-}\eta^1,\eta^1,\eta^2\text{-}C{\equiv}CR')_3]^+$ are mainly from the IL [π–π*] transitions of the C≡CR′ ligand.

The luminescence lifetimes of complexes **1**–**15** in the microsecond range indicate that both emissions originate from excited states of triplet parentage. Since the three highest occupied orbitals and lowest unoccupied orbitals are all close in their orbital energies, it is hard to predict which excitation would correspond to the lowest-energy excited state. In view of this, the lowest-energy triplet excited state was calculated by using time-dependent (TD) DFT based on the ground-state optimized geometry of **1a**. It has been found that this state is multiconfigurational, involving mainly [HOMO→LUMO], [HOMO−1→LUMO+1], and [HOMO−2→LUMO+2] excitations with transition coefficients of −0.32, −0.42, and 0.42, respectively. On the basis of the three main excitations in the $T_1$ state obtained from TD-DFT calculations, the unrestricted Kohn–Sham approach (UPBE1PBE) was used to optimize the three triplet excited states in order to determine the energy and relative ordering of the triplet excited states at relaxed molecular geometries.

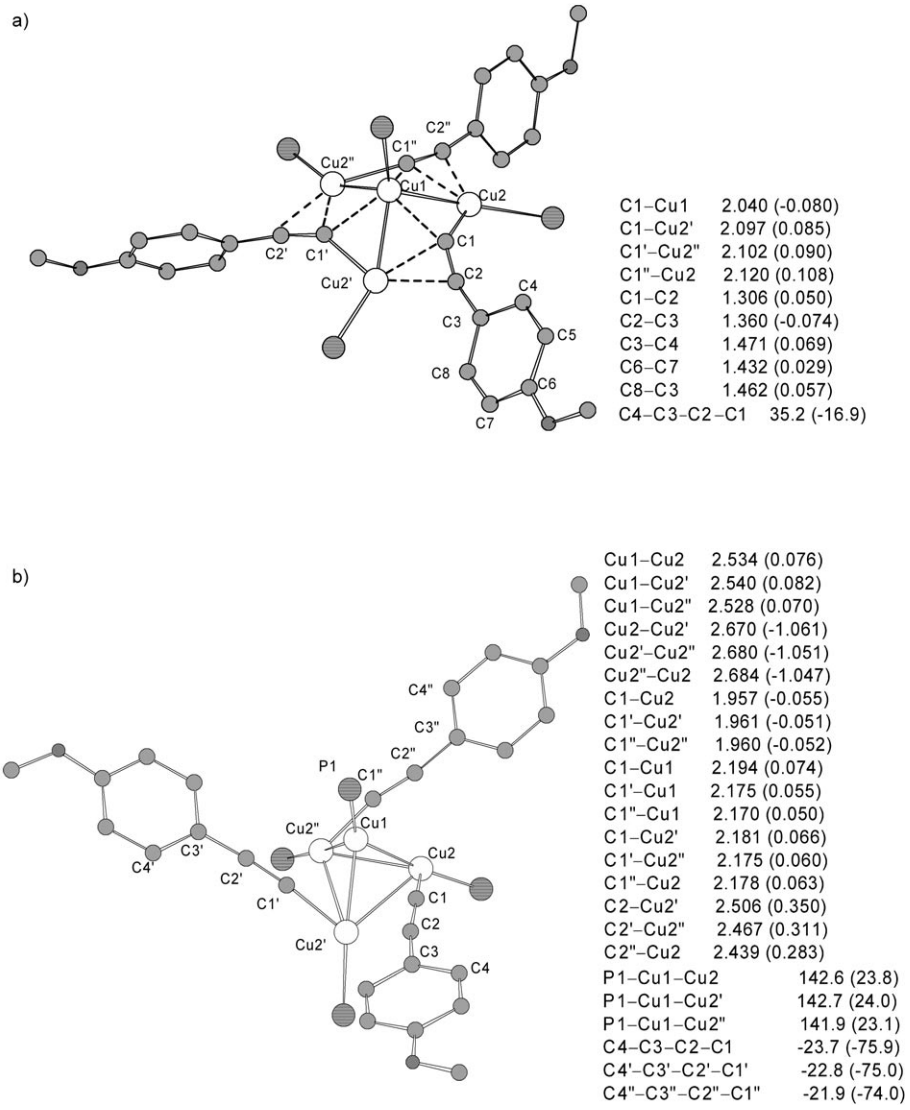


Figure 7. Selected structural parameters of the optimized a) [HOMO→LUMO] and b) [HOMO−2→LUMO+2] triplet excited states with the change in structural parameters with respect to the ground state in parentheses. Bond lengths and angles are in Å and °, respectively. Hydrogen atoms are omitted for simplicity.

The optimizations involving [HOMO→LUMO] excitation with no symmetry constraint display small geometrical changes, relative to that of the ground state. Figure 7a shows the optimized structure of the triplet state from [HOMO→LUMO] excitations and selected changes in the structural parameters relative to that of the ground state. The major geometrical changes occur mainly in one of the C≡C-*p*-$MeOC_6H_4$ units and some of the Cu−C bond lengths. Inspection of the two singly occupied molecular orbitals (SOMO) of the optimized triplet excited state from [HOMO→LUMO] excitation (Figure 8a) reveals that the lower- and higher-energy SOMOs are contributions mainly from π and π* orbitals of the C≡C-*p*-$MeOC_6H_4$ units, respectively, each with some participation from the metal orbitals. This provides a clear indication that the excited state contained the metal perturbed IL [π→π*(C≡C-*p*-$MeOC_6H_4$)] character. Attempts to optimize the excited state involving the [HOMO−1→LUMO+1] excitation failed. Optimization started with an initial guess for [HOMO−1→LUMO+1] excited state led to a geometry close to that obtained from the calculations based on the [HOMO→LUMO] excited state.

Optimization of the triplet state involving [HOMO−2→LUMO+2] excitation has led to a significant structural distortion relative to that of the ground state, and this excited state is slightly higher in energy than the $^3$IL [HOMO→LUMO] excited state by 2.3 kcal mol$^{-1}$.[12] Figure 7b illus-

  

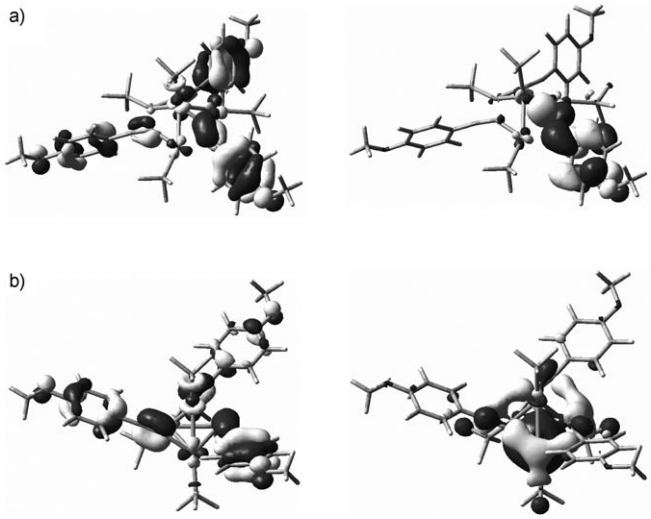


Figure 8. Spatial plots (isovalue = 0.03) of the lowest (left) and highest (right) SOMOs for **1a** at the optimized geometry of the a) [HOMO→LUMO] and b) [HOMO−2→LUMO+2] triplet excited states.

trates the optimized geometry of the triplet excited state of **1a** derived from [HOMO−2→LUMO+2] excitation. Such distortion is illustrated in Scheme 3 and can be described as

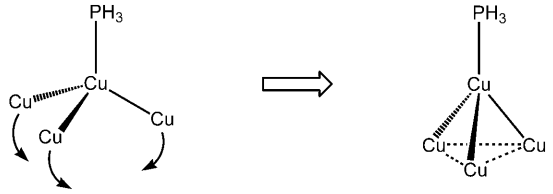


Scheme 3. Schematic diagram showing the "umbrella-opening" distortion (as under a strong wind) in the excited state of **1a** derived from the [HOMO−2→LUMO+2] excitation.

an "umbrella-opening" distortion (as under a strong wind), which has been previously discussed in tetracoordinate transition-metal complex distortions.[13] The central Cu1 atom is surrounded by one phosphine ligand and three peripheral copper atoms with side-on π-bonding coordination from the C≡C-*p*-MeOC$_6$H$_4$ units, forming a distorted Cu$_4$ tetrahedron. The excited-state structure is distorted in such a way that all the three P1−Cu1−Cu bond angles are opened up by 22.5–24.2° and the Cu···Cu distances within the bottom triangular face (ΔCu2–Cu2′–Cu2″) are significantly shortened by 1.047–1.061 Å (Figure 8b) relative to the ground-state geometry.

To understand the significant distortion in this excited state, the two SOMOs of the triplet state from [HOMO−2→LUMO+2] excitation are shown in Figure 8b. The lower-energy SOMO is mainly the contribution from the π orbitals of the C≡CAr units, with the metal orbitals contributing to a lesser extent. The higher-energy SOMO is mainly constituted of the in-phase combination of the sp-hybridized orbitals at the three peripheral Cu centers in the distorted trigonal-planar geometry, pointing outward from the bottom Cu$_3$ triangular face of the distorted Cu$_4$ tetrahedron, and the three π* orbitals of the three C≡C-*p*-MeOC$_6$H$_4$ ligands. The π orbitals at the α and β alkynyl carbon atoms have positive and negative overlaps with the in-phase combination, respectively, in this higher-energy SOMO, and a simplified bonding picture is given in Scheme 4. Upon the population of electron density in this orbital, it is expected that the three Cu−C$_\alpha$ bond lengths and Cu···Cu separations amongst ΔCu2–Cu2′–Cu2″ are shortened, whereas the Cu−C$_\beta$ bonds are lengthened, relative to those in the ground state (Figure 8b). Such results indicate that the triplet state derived from [HOMO−2→LUMO+2] excitation exhibits both the LMCT [π(C≡C-*p*-MeOC$_6$H$_4$)→4 s/p(Cu)] and MC [3d→4s/p(Cu)] characters, or alternatively, a $^3$LMCT excited state mixed with metal cluster-centered character ($^3$LMCT/$^3$MC), as both excitations would give rise to an excited-state structure with distortions mainly localized within the cluster core.

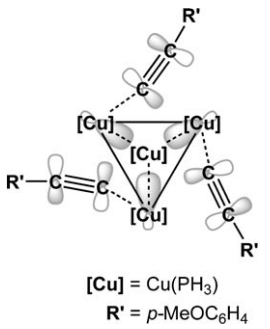


Scheme 4. Simple picture of the higher-energy SOMO in the [HOMO−2→LUMO+2] triplet excited state of **1a**.

The theoretical emission maxima of the $^3$IL and $^3$LMCT/$^3$MC triplet excited states of **1a**, estimated from the differences between the triplet- and ground-state energies at their corresponding excited-state equilibrium geometries, are 516 nm and 633 nm, respectively. These results match well with the high-energy emission band at 445 nm and low-energy emission band at 630 nm in **1** upon photoexcitation. Furthermore, the structural distortion energies of the $^3$IL and $^3$LMCT/$^3$MC states, which are calculated as the difference between the ground-state and excited state energies at the corresponding excited-state equilibrium geometries, are 10 and 23 kcal mol$^{-1}$, respectively. These indicate that the $^3$LMCT/$^3$MC excited state exhibits more significant structural distortion than that for the $^3$IL state, which is in good agreement with the observation of a larger Stokes shift in the low-energy emission band. Although the $^3$LMCT/$^3$MC state is slightly higher in energy than the $^3$IL state, the significant structural distortion presented at this $^3$LMCT/$^3$MC state relative to that of the ground state accounts for the observation of the low-energy emission derived from it. The more distorted $^3$LMCT/$^3$MC excited state could also account for the observed rigidochromism of the low-energy emission band, since a more rigid medium would certainly increase the energy of such a highly distorted excited state.

## Photochemical Properties

### *Oxidative Quenching Studies*

The photo-redox behavior of these tetranuclear copper(I) alkynyl complexes was also investigated. A study of elec-

  

tron-transfer quenching of the phosphorescent state of **1** by a series of structurally related pyridinium acceptors of variable reduction potentials, $E(A^{+/0})$, was carried out and communicated.[7] As the triplet-state energies of these pyridinium salts are too high for any appreciable energy-transfer reaction to occur, the quenching of the excited state of **1** most probably occurs through an electron-transfer mechanism. An excited-state reduction potential, $E^{o}[Cu_4(PPh_3)_4(\mu_3\text{-}\eta^1,\eta^1,\eta^2\text{-}C\equiv C\text{-}p\text{-}MeOC_6H_4)_3{}^{2+/+*}]$ of −1.71 V versus that of a saturated sodium chloride calomel electrode (SSCE) [$\lambda = 1.36$ eV] was estimated by a three-parameter, nonlinear least-squares fit to Equation (1),

$$\frac{RT}{F}\ln k_q' = \frac{RT}{F}\ln K\kappa\nu - \frac{\lambda}{4}\left[1+\left(\frac{\Delta G^{\circ\prime}}{\lambda}\right)\right]^2 \quad (1)$$

which was derived from the Marcus quadratic Equation (2),[14]

$$\Delta G^{\ddagger} = \frac{\lambda}{4}\left[1+\left(\frac{\Delta G^{\circ\prime}}{\lambda}\right)\right]^2 \quad (2)$$

where $k_q'$ is the rate constant corrected for the diffusional effects, $K = k_d/k_{-d}$ and is approximately 1–2 $dm^3 mol^{-1}$, $k_d$ is the diffusion-limited rate constant (taken to be $1.0\times10^{10}$ $dm^3 mol^{-1} s^{-1}$), $\kappa$ is the transmission coefficient, $\nu$ is the nuclear frequency, and $\lambda$ is the reorganization energy for electron transfer, $\Delta G^{\ddagger}$ is the free energy of activation, and $\Delta G^{o\prime}$ is the standard free energy change of the reaction corrected for work terms for association of reactants and dissociation of the products, which is given by Equation (3) for oxidative quenching,

$$\Delta G^{\circ} = E^{\circ}\left[Cu^{2+/+*}\right] - E^{\circ}(A^{+/0}) + w_r - w_p \quad (3)$$

where $w_r$ and $w_p$ are work terms for bringing the reactants and products to the mean separation for reaction. These work terms are usually very small and are neglected in the analysis of the electron-transfer-rate data. It is envisaged that **1** is a strong reductant in the excited state in view of its highly negative excited-state reduction potential. The close agreement between the experimental data and the prediction from the Marcus theory suggests that electron transfer is the predominant luminescence quenching mechanism of $[Cu_4(PPh_3)_4(\mu_3\text{-}\eta^1,\eta^1,\eta^2\text{-}C\equiv C\text{-}p\text{-}MeOC_6H_4)_3]^{+*}$ and pyridinium salts. This is consistent with the prediction that energy transfer does not contribute to a significant extent, as the triplet energies of the quenchers are too high for energy transfer to be competitive with electron-transfer quenching. Similar studies on **14** have also been performed, and Table 4 summarizes the associated bimolecular rate constants.[15]

Table 4. Bimolecular rate constants for the oxidative quenching of $[Cu_4\{P(p\text{-}MeC_6H_4)_3\}_4(\mu_3\text{-}\eta^1,\eta^1,\eta^2\text{-}C\equiv C\text{-}p\text{-}MeOC_6H_4)_3]^{+*}$ by pyridinium acceptors in degassed acetone (0.1 mol $dm^{-3}$ $nBu_4NPF_6$).

| Quencher[a] | $E(A^{+/0})$[b] [V vs. SSCE] | $k_q$ [$dm^3 mol^{-1} s^{-1}$] | $k_q'$[c] [$dm^3 mol^{-1} s^{-1}$] | $\ln k_q'$ |
|---|---|---|---|---|
| 4-cyano-*N*-methylpyridinium | −0.67 | $4.07\times10^9$ | $6.88\times10^9$ | 22.65 |
| 4-methoxycarbonyl-*N*-methylpyridinium | −0.78 | $3.92\times10^9$ | $6.46\times10^9$ | 22.59 |
| 4-aminoformyl-*N*-ethylpyridinium | −0.93 | $1.58\times10^9$ | $1.88\times10^9$ | 21.35 |
| 3-aminoformyl-*N*-methylpyridinium | −1.14 | $3.19\times10^8$ | $3.30\times10^8$ | 19.61 |
| *N*-ethylpyridinium | −1.36 | $6.29\times10^7$ | $6.33\times10^7$ | 17.96 |
| 4-methyl-*N*-methylpyridinium | −1.49 | $3.88\times10^6$ | $3.88\times10^6$ | 15.17 |

[a] All the compounds are hexafluorophosphate salts. [b] From reference [15]. [c] $(1/k_q') = (1/k_q) - (1/k_d)$ where $k_d$ is the diffusion-limited rate constant, taken to be $1.0\times10^{10}$ $dm^3 mol^{-1} s^{-1}$.

The excited-state reduction potential, $E^{o}[Cu_4\{P(p\text{-}MeC_6H_4)_3\}_4(\mu_3\text{-}\eta^1,\eta^1,\eta^2\text{-}C\equiv C\text{-}p\text{-}MeOC_6H_4)_3{}^{2+/+*}]$, was found to be −1.76 V versus that of the SSCE [$\lambda = 1.23$ eV]. A plot of $\ln k_q'$ versus $E^{o}(A^{+/0})$ for the oxidative quenching of $[Cu_4\{P(C_6H_4Me\text{-}p)_3\}_4(\mu_3\text{-}\eta^1,\eta^1,\eta^2\text{-}C\equiv C\text{-}p\text{-}MeOC_6H_4)_3]^{+*}$ is shown in Figure 9. It can be concluded that **14** is an even stronger reductant in the excited state than **1**, consistent with the fact that the presence of the more-strongly electron-donating tolyl groups in **14** than the phenyl rings in **1** increases the electron-richness of the copper(I) centers and hence results in a more-negative excited-state reduction potential.

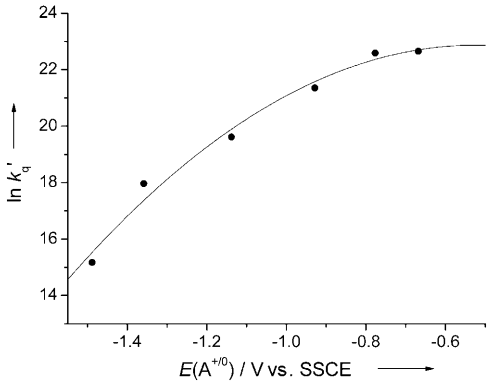


Figure 9. Plot of $\ln k_q'$ versus $E(A^{+/0})$ for the oxidative electron-transfer quenching of $[Cu_4\{P(p\text{-}MeC_6H_4)_3\}_4(\mu_3\text{-}\eta^1,\eta^1,\eta^2\text{-}C\equiv C\text{-}p\text{-}MeOC_6H_4)_3]^{+*}$ by pyridinium acceptors in degassed acetone (0.1 mol $dm^{-3}$ $nBu_4NPF_6$): (●) experimental; (——) theoretical.

*Transient Absorption Spectroscopy*

In order to establish the electron-transfer nature of this quenching reaction, nanosecond transient absorption spectroscopic study was carried out to provide direct spectroscopic evidence for such a mechanism. Laser flash photolysis of a degassed solution of **1** ($3.8\times10^{-5}$ mol $dm^{-3}$) in acetone (0.1 mol $dm^{-3}$ $nBu_4NPF_6$) with 4-methoxycarbonyl-*N*-methylpyridinium hexafluorophosphate ($5.0\times10^{-3}$ mol $dm^{-3}$) generated the transient absorption difference spectrum shown in Figure 10. It is dominated by two absorption bands, one at ≈400 nm, and a lower-intensity broad absorption band at

  

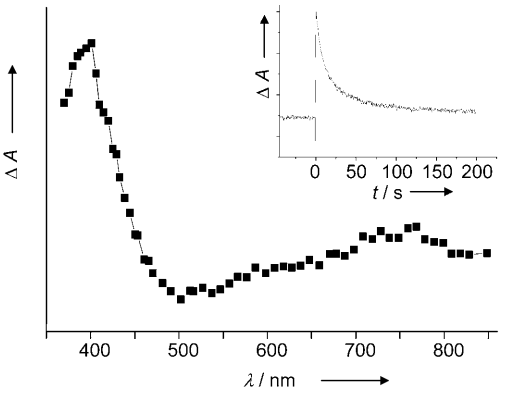


Figure 10. Transient absorption difference spectrum recorded 2 μs after laser flash for the reaction of $[Cu_4(PPh_3)_4(\mu_3\text{-}\eta^1,\eta^1,\eta^2\text{-}C\equiv C\text{-}p\text{-}MeOC_6H_4)_3]^{+*}$ and 4-methoxycarbonyl-*N*-methylpyridinium in degassed acetone (0.1 mol dm$^{-3}$ $n$Bu$_4$NPF$_6$). The insert shows the decay trace of the pyridinyl radical at 400 nm.

≈750 nm. The high-energy absorption band is characteristic of the pyridinyl radical and matches well with the reported spectrum of the 4-methoxycarbonyl-*N*-methylpyridinyl radical.[16] The mechanism for the photoinduced reaction is proposed in Scheme 5.

The 750-nm absorption band was not typical of the pyridinyl radical, but should be characteristic of the one-electron oxidized form of the cluster, $[Cu^ICu^ICu^ICu^{II}(PPh_3)_4(\mu_3\text{-}\eta^1,\eta^1,\eta^2\text{-}C\equiv C\text{-}p\text{-}MeOC_6H_4)_3]^{2+}$. The extinction coefficient of the band was estimated to be ≈2800 dm$^3$ mol$^{-1}$ cm$^{-1}$, assuming that both $[Cu_4(PPh_3)_4(\mu_3\text{-}\eta^1,\eta^1,\eta^2\text{-}C\equiv C\text{-}p\text{-}MeOC_6H_4)_3]^{+}$ and $[Cu_4(PPh_3)_4(\mu_3\text{-}\eta^1,\eta^1,\eta^2\text{-}C\equiv C\text{-}p\text{-}MeOC_6H_4)_3]^{2+}$ do not undergo significant absorption at ≈400 nm. A probable assignment for this absorption is the intervalence-transfer (IT) transition:

$$Cu^ICu^ICu^ICu^{II} \quad + \quad h\nu \quad \rightarrow \quad Cu^ICu^ICu^{II}Cu^{I*}$$

There have been a number of reports on the observation of intervalence-transfer transitions in a variety of mixed-valence copper(I,II) systems. For example, the 756-nm absorption band ($\varepsilon = 5000$ dm$^3$ mol$^{-1}$ cm$^{-1}$) of a dinuclear complex $[Cu^ICu^{II}L]^{3+}$ with a macrocyclic ligand L = N(CH$_2$CH$_2$N=C–C=NCH$_2$CH$_2$)$_3$N has been assigned as an intervalence-transfer transition.[17a] A similar assignment was also suggested in other mixed-valence $Cu^ICu^{II}$ systems with thiolato,[17b] halo[17c], and other N,O-containing macrocyclic ligands.[17d,e] Similar low-energy transient-absorption bands in the near-infrared region for the mixed-valence copper species were also observed in the photoinduced electron-transfer reactions of a series of trinuclear alkynylcopper(I) and tetranuclear copper(I) chalcogenido complexes with various pyridinium acceptors by using nanosecond transient absorption difference spectroscopy, and their origin was attributed to IT transitions.[5a,c,18]

Furthermore, the transient absorption spectroscopic studies can also provide important information on the back-electron-transfer (bet) reaction. The decay trace of the 400-nm absorption band, which is due to the absorptions of the pyridinyl radical, displayed absorption signals that returned to the baseline eventually, indicative of no substantial side reactions, other than that of back electron transfer (inset in Figure 10). A plot of $[1/\Delta A]$ versus time gave a straight line (Figure 11), indicating that the decay followed second-order

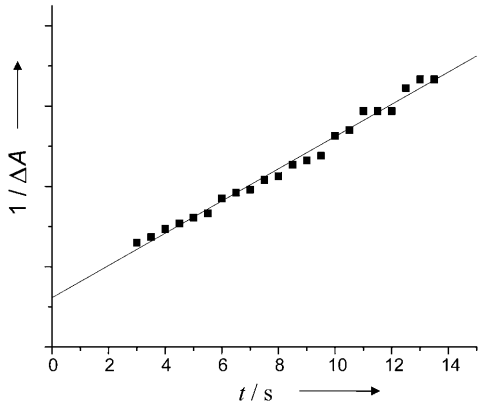


Figure 11. Plot of $(1/\Delta A)$ versus time at 400 nm for the reaction of $[Cu_4(PPh_3)_4(\mu_3\text{-}\eta^1,\eta^1,\eta^2\text{-}C\equiv C\text{-}p\text{-}MeOC_6H_4)_3]^{+*}$ and 4-methoxycarbonyl-*N*-methylpyridinium in degassed acetone (0.1 mol dm$^{-3}$ $n$Bu$_4$NPF$_6$).

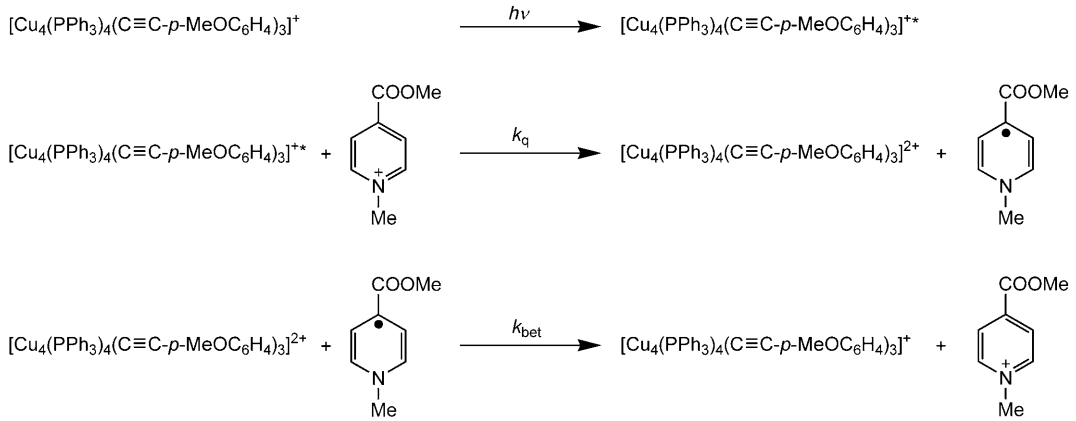


Scheme 5. Photoinduced oxidative electron-transfer mechanism for the reaction of **1** with 4-methoxycarbonyl-*N*-methylpyridinium acceptor.

  

CHEMISTRY
AN ASIAN JOURNAL

kinetics. The back-electron-transfer rate constant, $k_{bet}$, can be determined from Equation (4).

$$k_{bet} = b\, m\, \Delta\varepsilon \quad (4)$$

The path length $b$ of the optical cell is 0.4 cm, $m$ is the slope of the straight line obtained from the plot $[1/\Delta A]$ versus time, and $\Delta\varepsilon = \Sigma\varepsilon_{products} - \Sigma\varepsilon_{reactants}$. A $k_{bet}$ value of $1.0 \times 10^7\ dm^3\,mol^{-1}\,s^{-1}$ was determined on the basis of the decay of the mixed-valence species, and this value agrees well with that obtained from the $Cu^ICu^ICu^ICu^{II}$ mixed-valence species decay trace at 750 nm.

Similar transient absorption difference spectra were also observed for the photoinduced electron-transfer reaction between **1** and methyl viologen ($MV^{2+}$) hexafluorophosphate (Figure 12). The spectrum is dominated by two absorption

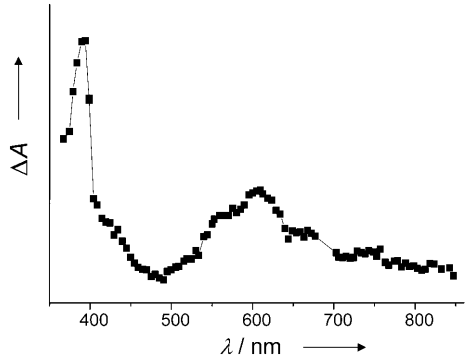


Figure 12. Transient absorption difference spectrum recorded 2 μs after laser flash for the reaction of $[Cu_4(PPh_3)_4(\mu_3\text{-}\eta^1,\eta^1,\eta^2\text{-}C\equiv C\text{-}p\text{-}MeOC_6H_4)_3]^{+*}$ and methyl viologen in degassed acetone (0.1 mol dm$^{-3}$ $n$Bu$_4$NPF$_6$).

bands, one sharp band at ≈400 nm and a broad band at ≈605 nm. Both are attributable to the reduced methyl viologen radical based on its reported spectrum.[19] The expected absorption band of the mixed-valence $Cu^ICu^ICu^ICu^{II}$ species was not clearly observed and might be obscured by the intense absorption of $MV^{+\cdot}$.

## Conclusions

A novel class of tetranuclear copper(I) alkynyl complexes with an "open-cube" structure was synthesized, and the crystal structure of $[Cu_4\{P(p\text{-}MeC_6H_4)_3\}_4(\mu_3\text{-}\eta^1,\eta^1,\eta^2\text{-}C\equiv C\text{-}p\text{-}MeOC_6H_4)_3]PF_6$ was determined. These complexes display dual-emission behavior. Through systematic comparison studies of the electronic absorption and photoluminescence properties of a series of $[Cu_4(PR_3)_4(\mu_3\text{-}\eta^1,\eta^1,\eta^2\text{-}C\equiv CR')_3]^+$, together with density functional theory calculations at the PBE1PBE level on the model complex $[Cu_4(PH_3)_4(\mu_3\text{-}\eta^1,\eta^1,\eta^2\text{-}C\equiv C\text{-}p\text{-}MeOC_6H_4)_3]^+$, the nature of their emission origins was probed. Their photochemical properties were also investigated by oxidative-quenching experiments and transient-absorption spectroscopy.

## Experimental Section

*Materials and Reagents*

Potassium tetrachloroaurate(III) and *trans*-dichlorobis(triphenylphosphine)palladium(II) were obtained from Strem Chemicals Inc. All the substituted phenylacetylenes were obtained from Maybridge Chemical Company, Ltd. $[Cu(MeCN)_4]PF_6$,[20] 2-ethynylthiophene,[21] and $[Au(C\equiv CR)]_\infty$[22] were prepared according to literature procedures. All solvents were purified and distilled under a nitrogen atmosphere by using standard procedures prior to use. All other reagents were of analytical grade and were used as received. The pyridinium salts for quenching studies were prepared by heating the corresponding pyridine and alkylating agent in acetone/ethanol (1:1 *v*/*v*) at reflux for 4 h, followed by a metathesis reaction with ammonium hexafluorophosphate in water, and subsequent recrystallization from acetonitrile/diethyl ether. Tetra-*n*-butylammonium hexafluorophosphate (Aldrich) was recrystallized three times from hot ethanol and dried under vacuum for 24 h prior to use.

*Physical Measurements and Instrumentation*

$^1$H NMR spectra were recorded on a Bruker DPX-300 (300 MHz) FT-NMR spectrometer, with chemical shifts ($\delta$, ppm) reported relative to $Me_4Si$ (TMS). Elemental analyses of all the newly synthesized metal complexes were performed either at the Butterworth Laboratories Ltd. or on a Carlo Erba 1106 elemental analyzer at the Institute of Chemistry, the Chinese Academy of Sciences in Beijing. All positive-ion FAB and electrospray ionization (ESI) mass spectra were recorded on Finnigan MAT95 and Finnigan LCQ mass spectrometers, respectively. All electronic absorption spectra were recorded on a Hewlett–Packard 8452 A diode array spectrophotometer. Steady-state emission and excitation spectra recorded at room temperature and at 77 K were obtained on a Spex Fluorolog-2 Model F111 fluorescence spectrophotometer with or without corning filters. All solutions for photophysical studies were prepared in a two-compartment cell consisting of a 10-cm$^3$ Pyrex bulb equipped with a side-arm to a 1-cm-pathlength quartz cuvette, and sealed from the atmosphere by a Rotaflo HP6/6 quick-release Teflon stopper. Solutions were degassed under high vacuum (limiting pressure $<10^{-3}$ torr) with no less than four successive freeze–pump–thaw cycles. Solid-state photophysical measurements were carried out with solid samples loaded in a quartz tube inside a quartz-walled Dewar flask. Liquid nitrogen was placed in the Dewar flask for low-temperature (77 K) solid-state and glass photophysical measurements. Emission lifetime measurements were performed with a conventional laser system. The excitation source was the 355-nm-output (third harmonic) of a Spectra-Physics Quanta-Ray Q-switched GCR-150-10 pulsed Nd-YAG laser. Luminescence decay signals were recorded on a Tektronix model TDS620 A digital oscilloscope, and analyzed by using a program for exponential fits.

*Syntheses*

All reactions were carried out by using standard Schlenk techniques under an inert atmosphere of nitrogen.

**1**:[7] $[Cu(MeCN)_4]PF_6$ (0.10 g, 0.27 mmol) was suspended in dichloromethane (20 mL), and triphenylphosphine (0.21 g, 0.81 mmol) was added. Stirring was continued until the triphenylphosphine dissolved completely. $[Au(C\equiv C\text{-}p\text{-}MeOC_6H_4)]_\infty$ (88 mg, 0.27 mmol) was added, and the yellow suspension changed rapidly into a clear yellow solution. Stirring was continued for 15 min, and the resulting solution was filtered. The volume of the filtrate was decreased under reduced pressure, followed by diffusion of diethyl ether vapor into the preconcentrated solution of the complex in dichloromethane to yield **1** as air-stable pale-yellow crystals. Yield: 85 mg (69%). IR (Nujol): $\tilde{\nu}$ = 842 cm$^{-1}$ (s, ν(P-F)); $^1$H NMR (300 MHz, [D$_6$]acetone, 298 K, TMS): $\delta$ = 3.71 (s, 9H; $OCH_3$), 6.38 (d, $^3J$(H,H) = 10 Hz, 6H; $C\equiv CC_6H_4$), 6.48 (d, $^3J$(H,H) = 10 Hz, 6H; $C\equiv CC_6H_4$), 7.10–7.38 ppm (m, 60H; $PPh_3$); MS (positive-ion FAB): *m*/*z*: 1696 $[M-PF_6]^+$;

  

elemental analysis: calcd (%) for $C_{99}H_{81}Cu_4F_6O_3P_5 \cdot {}^1/_2CH_2Cl_2$ (1884.2): C 63.42, H 4.35; found: C 63.42, H 4.46.

**2:** The procedure was similar to that used in the preparation of **1**, except that $[Au(C\equiv C\text{-}p\text{-}EtOC_6H_4)]_\infty$ (92 mg, 0.27 mmol) was used instead of $[Au(C\equiv C\text{-}p\text{-}MeOC_6H_4)]_\infty$, yielding **2** as air-stable pale-yellow crystals (90 mg, 56%). IR (KBr): $\tilde{\nu}=842\ cm^{-1}$ (s, ν(P-F)); $^1H$ NMR (300 MHz, $CDCl_3$, 298 K, TMS): $\delta=1.37$ (t, $^3J(H,H)=6.9$ Hz, 9H; $CH_3$), 3.89 (q, $^3J(H,H)=6.9$ Hz, 6H; $OCH_2$), 6.24–6.32 (m, 12H; $C_6H_4$), 7.01–7.23 ppm (m, 60H; $PPh_3$); MS (positive-ion FAB): *m/z*: 1737 $[M-PF_6+H]^+$; MS (positive ESI): *m/z*: 1736 $[M-PF_6]^+$; elemental analysis: calcd (%) for $C_{102}H_{87}Cu_4F_6O_3P_5 \cdot CH_2Cl_2$ (1968.8): C 62.84, H 4.56; found: C 62.94, H 4.79.

**3**: The procedure was similar to that used in the preparation of **1** except that $[Au(C\equiv C\text{-}p\text{-}nBuOC_6H_4)]_\infty$ (100 mg, 0.27 mmol) was used instead of $[Au(C\equiv C\text{-}p\text{-}MeOC_6H_4)]_\infty$, yielding **3** as air-stable pale-yellow crystals (93 mg, 53%). IR (KBr): $\tilde{\nu}=841\ cm^{-1}$ (s, ν(P-F)); $^1H$ NMR (300 MHz, $CDCl_3$, 298 K, TMS): $\delta=0.97$ (t, $^3J(H,H)=7.3$ Hz, 9H; $CH_3$), 1.43–1.48 (m, 6H; $CH_2CH_3$), 1.72–1.76 (m, 6H; $OCH_2CH_2$), 3.81 (t, $^3J(H,H)=$ 6,5 Hz, 6H; $OCH_2$), 6.24–6.32 (m, 12H; $C_6H_4$), 6.99–7.22 ppm (m, 60H; $PPh_3$); MS (positive-ion FAB): *m/z*: 1559 $[M-PF_6-PPh_3]^+$; MS (positive ESI): *m/z*: 1821 $[M-PF_6]^+$; elemental analysis: calcd (%) for $C_{108}H_{99}Cu_4F_6O_3P_5 \cdot 1/5\ CH_2Cl_2$ (1985.0): C 65.47, H 5.05; found: C 65.47, H 5.08.

**4**: The procedure was similar to that used in the preparation of **1**, except that $[Au(C\equiv C\text{-}p\text{-}nHexOC_6H_4)]_\infty$ (107 mg, 0.27 mmol) was used instead of $[Au(C\equiv C\text{-}p\text{-}MeOC_6H_4)]_\infty$, yielding **4** as air-stable pale-yellow crystals (100 mg, 54%). IR (KBr): $\tilde{\nu}=841\ cm^{-1}$ (s, ν(P-F)); $^1H$ NMR (300 MHz, $CDCl_3$, 298 K, TMS): $\delta=0.91$ (t, $^3J(H,H)=6.7$ Hz, 9H; $CH_3$), 1.18–1.45 (m, 18H; $CH_2CH_2CH_2CH_3$), 1.68–1.75 (m, 6H; $OCH_2CH_2$), 3.80 (t, $^3J(H,H)=6.5$ Hz, 6H; $OCH_2$), 6.24–6.32 (m, 12H; $C_6H_4$), 7.01–7.22 ppm (m, 60H; $PPh_3$); MS (positive-ion FAB): *m/z* : 1906 $[M-PF_6+H]^+$; MS (positive ESI): *m/z*: 1905 $[M-PF_6]^+$; elemental analysis: calcd (%) for $C_{114}H_{111}Cu_4F_6O_3P_5 \cdot CH_2Cl_2$ (2137.1): C 64.63, H 5.33; found: C 64.41, H 5.26.

**5**: The procedure was similar to that used in the preparation of **1**, except that $[Au(C\equiv C\text{-}p\text{-}nHeptOC_6H_4)]_\infty$ (111 mg, 0.27 mmol) was used instead of $[Au(C\equiv C\text{-}p\text{-}MeOC_6H_4)]_\infty$, yielding **5** as air-stable pale-yellow crystals (105 mg, 56%). IR (KBr): $\tilde{\nu}=841\ cm^{-1}$ (s, ν(P-F)); $^1H$ NMR (300 MHz, $CDCl_3$, 298 K, $Me_4Si$): $\delta=0.89$ (t, $^3J(H,H)=6.9$ Hz, 9H; $CH_3$), 1.23–1.42 (m, 6H; $CH_2CH_3$), 1.68–1.75 (m, 24H; $OCH_2CH_2CH_2CH_2CH_2$), 3.82 (t, $^3J(H,H)=6.5$ Hz, 6H; $OCH_2$), 6.24–6.32 (m, 12H; $C_6H_4$), 6.98–7.30 ppm (m, 60H; $PPh_3$); MS (positive-ion FAB): *m/z*: 1685 $[M-PPh_3-PF_6+H]^+$; MS (positive ESI): *m/z*: 1945 $[M-PF_6]^+$; elemental analysis: calcd (%) for $C_{117}H_{117}Cu_4F_6O_3P_5 \cdot 5/4\ CH_2Cl_2$ (2200.4): C 64.55, H 5.47; found: C 64.57, H 5.25.

**6**: The procedure was similar to that used in the preparation of **1**, except that $[Au(C\equiv C\text{-}p\text{-}MeC_6H_4)]_\infty$ (84 mg, 0.27 mmol) was used instead of $[Au(C\equiv C\text{-}p\text{-}MeOC_6H_4)]_\infty$, yielding **6** as air-stable pale-yellow crystals (87 mg, 72%). IR (nujol): $\tilde{\nu}=840\ cm^{-1}$ (s, ν(P-F)); $^1H$ NMR (300 MHz, $[D_6]$acetone, 298 K, TMS): $\delta=2.19$ (s, 9H; $CH_3$), 6.42 (d, $^3J(H,H)=9$ Hz, 6H; $C\equiv CC_6H_4$), 6.64 (d, $^3J(H,H)=9$ Hz, 6H; $C\equiv CC_6H_4$), 7.06–7.38 ppm (m, 60H; $PPh_3$); MS (positive-ion FAB): *m/z*: 1646 $[M-PF_6+H]^+$; MS (positive ESI): *m/z*: 1646 $[M-PF_6+H]^+$; elemental analysis: calcd (%) for $C_{99}H_{81}Cu_4F_6P_5$ (1793.7): C 66.29, H 4.55; found: C 65.94, H 4.57.

**7**: The procedure was similar to that used in the preparation of **1**, except that $[Au(C\equiv C\text{-}p\text{-}nBuC_6H_4)]_\infty$ (96 mg, 0.27 mmol) was used instead of $[Au(C\equiv C\text{-}p\text{-}MeOC_6H_4)]_\infty$, yielding **7** as air-stable pale-yellow crystals (83 mg, 48%). IR (KBr): $\tilde{\nu}=839\ cm^{-1}$ (s, ν(P-F)); $^1H$ NMR (300 MHz, $CDCl_3$, 298 K, TMS): $\delta=0.90$ (t, $^3J(H,H)=7.3$ Hz, 9H; $CH_3$), 1.27–1.32 (m, 6H; $CH_2CH_3$), 1.40–1.50 (m, 6H; $CH_2CH_2CH_3$), 2.42 (t, $^3J(H,H)=$ 7.6 Hz, 6H; $C_6H_4CH_2$), 6.30 (d, $^3J(H,H)=8.0$ Hz, 6H; $C_6H_4$), 6.57 (d, $^3J(H,H)=8.0$ Hz, 6H; $C_6H_4$), 7.02–7.23 ppm (m, 60H; $PPh_3$); MS (positive-ion FAB): *m/z*: 1511 $[M-PPh_3-PF_6+H]^+$; MS (positive ESI): *m/z* 1772 $[M-PF_6]^+$; elemental analysis: calcd (%) for $C_{108}H_{99}Cu_4F_6P_5 \cdot CH_2Cl_2$ (2004.9): C 65.30, H 5.08; found: C 65.08, H 5.12.

**8**: The procedure was similar to that used in the preparation of **1**, except that $[Au(C\equiv C\text{-}p\text{-}nHexC_6H_4)]_\infty$ (103 mg, 0.27 mmol) was used instead of $[Au(C\equiv C\text{-}p\text{-}MeOC_6H_4)]_\infty$, yielding **8** as air-stable pale-yellow crystals (84 mg, 47%). IR (KBr): $\tilde{\nu}=840\ cm^{-1}$ (s, ν(P-F)); $^1H$ NMR (300 MHz, $CDCl_3$, 298 K, TMS): $\delta=0.87$ (t, $^3J(H,H)=6.5$ Hz, 9H; $CH_3$), 1.18–1.25 (m, 18H; $CH_2CH_2CH_2CH_3$), 1.44–1.48 (m, 6H; $C_6H_4CH_2CH_2$), 2.40 (t, $^3J(H,H)=7.5$ Hz, 6H; $C_6H_4CH_2$), 6.30 (d, $J=7.9$ Hz, 6H; $C_6H_4$), 6.57 (d, $^3J(H,H)=7.9$ Hz, 6H; $C_6H_4$), 7.05–7.23 ppm (m, 60H; $PPh_3$); MS (positive-ion FAB): *m/z*: 1595 $[M-PPh_3-PF_6+H]^+$; MS (positive ESI): *m/z*: 1857 $[M-PF_6+H]^+$; elemental analysis: calcd (%) for $C_{114}H_{111}Cu_4F_6P_5 \cdot {}^3/_4CH_2Cl_2$ (2067.8): C 66.65, H 5.48; found: C 66.45, H 5.27.

**9**: The procedure was similar to that used in the preparation of **1**, except that $[Au(C\equiv C\text{-}p\text{-}nHeptC_6H_4)]_\infty$ (107 mg, 0.27 mmol) was used instead of $[Au(C\equiv C\text{-}p\text{-}MeOC_6H_4)]_\infty$, yielding **9** as air-stable pale-yellow crystals (86 mg, 47%). IR (KBr): $\tilde{\nu}=840\ cm^{-1}$ (s, ν(P-F)); $^1H$ NMR (300 MHz, $CDCl_3$, 298 K, TMS): $\delta=0.88$ (t, $^3J(H,H)=6.8$ Hz, 9H; $CH_3$), 1.32–1.36 (m, 24H; $CH_2CH_2CH_2CH_2CH_3$), 1.45–1.53 (m, 6H; $C_6H_4CH_2CH_2$), 2.41 (t, $^3J(H,H)=7.4$ Hz, 6H; $C_6H_4CH_2$), 6.29 (d, $^3J(H,H)=8.0$ Hz, 6H; $C_6H_4$), 6.57 (d, $^3J(H,H)=8.0$ Hz, 6H; $C_6H_4$), 6.92–7.22 ppm (m, 60H; $PPh_3$); MS (positive-ion FAB): *m/z*: 1637 $[M-PPh_3-PF_6+H]^+$; MS (positive ESI): *m/z*: 1899 $[M-PF_6+H]^+$; elemental analysis: calcd (%) for $C_{117}H_{117}Cu_4F_6P_5 \cdot {}^1/_2CH_2Cl_2$ (2088.7): C 67.57, H 5.69; found: C 67.68, H 5.67.

**10**: The procedure was similar to that used in the preparation of **1**, except that $[Au(C\equiv C\text{-}p\text{-}nOctC_6H_4)]_\infty$ (111 mg, 0.27 mmol) was used instead of $[Au(C\equiv C\text{-}p\text{-}MeOC_6H_4)]_\infty$, yielding **10** as air-stable pale-yellow crystals (92 mg, 49%). IR (KBr): $\tilde{\nu}=840\ cm^{-1}$ (s, ν(P-F)); $^1H$ NMR (300 MHz, $CDCl_3$, 298 K, TMS): $\delta=0.87$ (t, $^3J(H,H)=6.7$ Hz, 9H; $CH_3$), 1.18–1.25 (m, 30H, $CH_2CH_2CH_2CH_2CH_2CH_3$), 1.44–1.48 (m, 6H, $C_6H_4CH_2CH_2$), 2.38–2.43 (m, 6H; $C_6H_4CH_2$), 6.30 (d, $^3J(H,H)=8.0$ Hz, 6H; $C_6H_4$), 6.56 (d, $^3J(H,H)=8.0$ Hz, 6H; $C_6H_4$), 6.92–7.22 ppm (m, 60H; $PPh_3$); MS (positive-ion FAB): *m/z*: 1940 $[M-PF_6]^+$; MS (positive ESI): *m/z*: 1941 $[M-PF_6+H]^+$; elemental analysis: calcd (%) for $C_{120}H_{123}Cu_4F_6P_5 \cdot {}^1/_5CH_2Cl_2$ (2105.3): C 68.57, H 5.91; found (%): C 68.73, H 5.67.

**11**: The procedure was similar to that used in the preparation of **1**, except that $[Au(C\equiv C\text{-}p\text{-}C_6H_5C_6H_4)]_\infty$ (100 mg, 0.27 mmol) was used instead of $[Au(C\equiv C\text{-}p\text{-}MeOC_6H_4)]_\infty$, yielding **11** as pale-yellow crystals (93 mg, 70%). IR (Nujol): $\tilde{\nu}=837\ cm^{-1}$ (s, ν(P-F)); $^1H$ NMR (300 MHz, $[D_6]$acetone, 298 K, TMS): $\delta=6.49$ (d, $^3J(H,H)=9$ Hz, 6H; $C\equiv CC_6H_4$), 6.94 (d, $^3J(H,H)=9$ Hz, 6H; $C\equiv CC_6H_4$), 6.97–7.39 ppm (m, 75H; $C_6H_5$); MS (positive-ion FAB): *m/z*: 1836 $[M-PF_6+H]^+$; MS (positive ESI): *m/z*: 1835 $[M-PF_6]^+$; elemental analysis: calcd (%) for $C_{114}H_{87}Cu_4F_6P_5$ (1980.0): C 69.15, H 4.43; found: C 69.38, H 4.37.

**12**: The procedure was similar to that for **1**, except that $[Au(C\equiv C\text{-}p\text{-}ClC_6H_4)]_\infty$ (89 mg, 0.27 mmol) was used instead of $[Au(C\equiv C\text{-}p\text{-}MeOC_6H_4)]_\infty$, yielding **12** as pale-yellow crystals (92 mg, 74%). IR (nujol): $\tilde{\nu}=837\ cm^{-1}$ (s, ν(P-F)); $^1H$ NMR (300 MHz, $[D_6]$acetone, 298 K, TMS): $\delta=6.52$ (d, $^3J(H,H)=9$ Hz, 6H; $C\equiv CC_6H_4$), 6.78 (d, $^3J(H,H)=9$ Hz, 6H; $C\equiv CC_6H_4$), 7.10–7.44 ppm (m, 60H; $PPh_3$); MS (positive-ion FAB): *m/z*: 1710 $[M-PF_6+H]^+$; MS (positive ESI): *m/z*: 1709 $[M-PF_6]^+$; elemental analysis: calcd (%) for $C_{96}H_{72}Cu_4Cl_3F_6P_5 \cdot {}^1/_4CH_2Cl_2$ (1876.2): C 61.61, H 3.89; found C 61.68, H 3.81.

**13**: The procedure was similar to that used in the preparation of **1**, except that $[Au(C\equiv CC_4H_3S)]_\infty$ (82 mg, 0.27 mmol) was used instead of $[Au(C\equiv C\text{-}p\text{-}MeOC_6H_4)]_\infty$, yielding **13** as air-stable pale-yellow crystals (75 mg, 47%). IR (KBr): $\tilde{\nu}=838\ cm^{-1}$ (s, ν(P-F)); $^1H$ NMR (300 MHz, $CDCl_3$, 298 K, TMS): $\delta=6.04$ (dd, $^3J(H,H)=1.2$, 4.3 Hz, 3H; 3-thienyl protons), 6.44 (dd, $^3J(H,H)=4.3$, 5.1 Hz, 3H; 4-thienyl protons), 6.82 (dd, $^3J(H,H)=1.2$, 5.1 Hz, 3H; 5-thienyl protons), 7.10–7.23 ppm (m, 60H; $PPh_3$); MS (positive-ion FAB): *m/z*: 1623 $[M-PF_6]^+$; MS (positive ESI): *m/z*: 1623 $[M-PF_6]^+$; elemental analysis: calcd (%) for $C_{90}H_{69}Cu_4F_6P_5S_3 \cdot CH_2Cl_2$ (1854.7): C 58.93, H 3.86; found: C 58.65, H 3.69.

**14**: The procedure was similar to that used in the preparation of **1**, except that tri(*p*-tolyl)phosphine (0.21 g, 0.81 mmol) was used instead of triphenylphosphine, yielding **14** as air-stable pale-yellow crystals (123 mg, 51%). IR (KBr): $\tilde{\nu}=843\ cm^{-1}$ (s, ν(P-F)); $^1H$ NMR (300 MHz, $CDCl_3$, 298 K, TMS): $\delta=2.18$ (s, 36H; $CH_3$), 3.68 (s, 9H; OMe), 6.16 (d, $^3J(H,H)=8.7$ Hz, 6H; $C_6H_4O$), 6.30 (d, $^3J(H,H)=8.7$ Hz, 6 H $C_6H_4O$),

  

6.74–6.77 (m, 24H, $C_6H_4$), 6.94–6.98 ppm (m, 24H; $C_6H_4$). MS (positive-ion FAB): $m/z$: 1865 $[M-PF_6]^+$; MS (positive ESI): $m/z$: 1865 $[M-PF_6]^+$; elemental analysis: calcd (%) for $C_{111}H_{105}Cu_4F_6O_3P_5$ (2010.1): C 66.33, H 5.27; found: C 66.05, H 5.27.

**15**: The procedure was similar to that used in the preparation of **1**, except that P(*p*-$CF_3C_6H_4)_3$ (0.38 g, 0.81 mmol) was used instead of triphenylphosphine, yielding **15** as air-stable pale-yellow crystals (120 mg, 50%). IR (KBr): $\tilde{\nu}=838\ cm^{-1}$ (s, ν(P-F)); $^1H$ NMR (300 MHz, $CDCl_3$, 298 K, TMS): $\delta=3.59$ (s, 9H; OMe), 6.13 (d, $^3J(H,H)=8.8$ Hz, 6H; $C_6H_4O$), 6.61 (d, $^3J(H,H)=8.8$ Hz, 6H; $C_6H_4O$), 7.30–7.34 ppm (m, 48H; *p*-$CF_3C_6H_4$); MS (positive-ion FAB): $m/z$: 1980 $[M-Cu-P(C_6H_4CF_3)_3-PF_6]^+$; MS (positive ESI): $m/z$: 1577 $[M-2P(C_6H_4CF_3)_3-PF_6]^+$; elemental analysis: calcd (%) for $C_{111}H_{69}Cu_4F_{42}O_3P_5\cdot CH_2Cl_2$ (2742.7): C 49.05, H 2.61; found: C 49.10, H 2.53.

*Crystal-Structure Determination*

A pale yellow crystal of **14** of dimensions $0.40\times0.40\times0.15\ mm^3$, obtained by recrystallization from dichloromethane/diethyl ether, was mounted in a glass capillary and was used for data collection at 28°C on a MAR diffractometer with a 300-mm image plate detector with graphite-monochromated $Mo_{K\alpha}$ radiation ($\lambda=0.71073$ Å). Data collection was made with 2° oscillation steps of $\phi$, 300-s exposure time, and scanner distance at 120 mm. 101 images were collected. The copper and most of the non-H atoms were located according to the direct methods. The positions of the other non-hydrogen atoms were found after successful refinement by full-matrix least-squares using program SHELXL-97 on PC.[23] The O atom of a water molecule was located at a special position. According to the SHELXL-97 program,[23] all 15613 independent reflections ($R_{int}=0.0508$, 9401 reflections larger than $4\sigma(F_o)$) from a total of 48264 reflections were included in the full-matrix least-squares refinement against $F^2$. These reflections were in the range $h$: −18 to 18; $k$: −35 to 35; $l$: −27 to 26 with $2\theta_{max}=51.00°$. One crystallographic asymmetric unit consists of one formula unit, inclusive of one half of a water molecule. In the final stage of least-squares refinement, all non-hydrogen atoms were refined anisotropically. H atoms (except those on the O atom of water molecules) were generated by the program SHELXL-97.[23] The positions of the H atoms were calculated based on the riding mode with thermal parameters equal to 1.2 times that of the associated C atoms, and included in the calculation of final $R$ indices. $(\Delta/\sigma)_{max}=0.003$, av. 0.001 for 1136 variable parameters by full-matrix least-squares refinement on $F^2$ leads to $R_1=0.0547$ and $wR_2=0.1584$ with a goodness-of-fit of 0.942, the parameters $a$ and $b$ for the weighting scheme are 0.1131 and 0.0. The final difference Fourier map shows maximum rest peaks and holes of 1.782 and $-0.736\ e\ Å^{-3}$, respectively. CCDC-298052 contains the supplementary crystallographic data for this paper. These data can be obtained free of charge at www.ccdc.cam.ac.uk/data_request.cif.

*Computational Details*

Calculations were carried out with the Gaussian03 software package.[24] Density functional theory (DFT) at the hybrid Perdew, Burke, and Ernzerhof functional (PBE1PBE) level[25] was used to optimize the singlet ground-state ($S_0$) geometries of the model complex, $[Cu_4(PH_3)_4(\mu_3\text{-}\eta^1,\eta^1,\eta^2\text{-}C\equiv C\text{-}p\text{-}MeOC_6H_5)_3]^+$ (**1a**), with the constraint of $C_3$ symmetry. The Stuttgart/Dresden effective core potentials (ECPs)[26] on Cu were used to replace the inner core electrons, while the SDD basis set[27] was applied to describe the outer core ($3s^23p^6$) and the valence 3d electrons. To increase the accuracy, an f polarization function ($\zeta_f(Cu)=3.525$) was employed for Cu.[28] For all the other atoms (P, C, H, and O), the 6–31G(d) basis set[29] was used. Time-dependent (TD) DFT (PBE1PBE) was employed to calculate the lowest-energy triplet excited state based on the ground-state optimized geometry, by using the same basis set with PBE1PBE functional. On the basis of the three excitations in the first excited state from the TD-DFT calculation, geometry optimizations for the three triplet excited states in **1a** without symmetry constraints were performed by using unrestricted UPBE1PBE. Vibrational frequencies were calculated for all optimized geometries to verify that each was a minimum on the potential energy surface.

## Acknowledgements

V.W.-W.Y. acknowledges support from the University Development Fund (UDF) of the University of Hong Kong, the URC Seed Funding for Strategic Research Theme on Organic Optoelectronics, and the University of Hong Kong Foundation for Educational Development and Research Limited. The work described in this paper was supported by a Central Allocation Vote (CAV) Grant from the Research Grants Council of the Hong Kong Special Administrative Region, China (Project No. HKU 2/05C). C.-L.C. and K.-L.C. acknowledge the receipt of postgraduate studentships, and W.H.L. the support of a University Postdoctoral Fellowship, both administered by the University of Hong Kong. We also thank Professor Zhenyang Lin from the Hong Kong University of Science and Technology for his helpful discussion on the theoretical studies, and the Computer Center at the University of Hong Kong for providing the computational resources.

[1] a) H. D. De Ahna, H. D. Hardt, *Z. Anorg. Allg. Chem.* **1972**, *387*, 61; b) H. D. Hardt, H. Gechnizdjani, *Z. Anorg. Allg. Chem.* **1973**, *397*, 23; c) H. D. Hardt, Z. Pierre, *Z. Anorg. Allg. Chem.* **1973**, *402*, 107; d) H. D. Hardt, A. Pierre, *Inorg. Chim. Acta* **1977**, *25*, L59; e) H. D. Hardt, H. J. Stoll, *Z. Anorg. Allg. Chem.* **1981**, *480*, 193; f) H. D. Hardt, H. J. Stoll, *Z. Anorg. Allg. Chem.* **1981**, *480*, 199.

[2] a) M. Radjaipour, D. Oelkrug, *Ber. Bunsen-Ges.* **1978**, *82*, 159–163; b) E. Eitel, D. Oelkrug, W. Hiller, J. Strahle, *Z. Naturforsch. B* **1980**, *35*, 1247.

[3] a) A. Vogler, H. Kunkely, *J. Am. Chem. Soc.* **1986**, *108*, 7211; b) P. C. Ford, A. Vogler, *Acc. Chem. Res.* **1993**, *26*, 220.

[4] a) P. C. Ford, E. Cariati, J. Bourassa, *Chem. Rev.* **1999**, *99*, 3625, and references therein; b) M. Vitale, W. E. Palke, P. C. Ford, *J. Phys. Chem.* **1992**, *96*, 8329.

[5] a) L. Naldini, F. DeMartin, M. Manassero, M. Sansoni, G. Rassu, M. A. Zoroddu, *J. Organomet. Chem.* **1985**, *279*, C42; b) M. P. Gamasa, J. Gimeno, E. Lastra, *J. Organomet. Chem.* **1988**, *346*, 277; c) J. Díez, M. P. Gamasa, J. Gimeno, E. Lastra, A. Aguirre, S. García-Granda, *Organometallics* **1991**, *10*, 380; d) J. Díez, M. P. Gamasa, J. Gimeno, E. Lastra, A. Aguirre, S. García-Granda, *Organometallics* **1993**, *12*, 2213; e) J. Díez, M. P. Gamasa, J. Gimeno, E. Lastra, A. Aguirre, S. García-Granda, *Organometallics* **1997**, *16*, 3684.

[6] a) V. W.-W. Yam, *Acc. Chem. Res.* **2002**, *35*, 555, and references therein; b) V. W.-W. Yam, W.-K. Lee, K.-K. Cheung, *J. Chem. Soc. Dalton Trans.* **1996**, 2335; c) V. W.-W. Yam, W. K.-M. Fung, K.-K. Cheung, *J. Cluster Sci.* **1999**, *10*, 37; d) W.-Y. Lo, C.-H. Lam, V. W.-W. Yam, N. Zhu, K.-K. Cheung, S. Fathallah, S. Messaoudi, B. Le Guennic, S. Kahlal, J.-F. Halet, *J. Am. Chem. Soc.* **2004**, *126*, 7300.

[7] V. W.-W. Yam, S. W.-K. Choi, C.-L. Chan, K.-K. Cheung, *Chem. Commun.* **1996**, 2067.

[8] a) C. L. Raston, A. H. White, *J. Chem. Soc. Dalton Trans.* **1976**, 2153; b) J. C. Dyason, P. C. Healy, L. M. Engelhardt, C. Pakawatchat, V. A. Patrick, C. L. Ratson, A. H. White, *J. Chem. Soc. Dalton Trans.* **1985**, 831; c) M. R. Churchill, W. J. Young, *Inorg. Chem.* **1979**, *18*, 1133; d) M. R. Churchill, K. L. Kalra, *Inorg. Chem.* **1974**, *13*, 1065; e) M. R. Churchill, K. L. Kalra, *Inorg. Chem.* **1974**, *13*, 1899; f) M. R. Churchill, B. G. DeBoer, S. J. Mendak, *Inorg. Chem.* **1975**, *14*, 2041.

[9] For examples, see: a) F. A. Cotton, Z. Dori, R. Llusar, W. Schwotzer, *Inorg. Chem.* **1986**, *25*, 3654; b) M. Martinez, B. L. Ooi, A. G. Sykes, *J. Am. Chem. Soc.* **1987**, *109*, 4615; c) E. K. H. Roth, J. Jordanov, *Inorg. Chem.* **1992**, *31*, 240.

[10] a) A. Eichhöfer, D. Fenske, W. Holstein, *Angew. Chem.* **1993**, *105*, 257; *Angew. Chem. Int. Ed. Engl.* **1993**, *32*, 242; b) D. J. Brauer, G. Hessler, P. C. Knüppel, O. Stelzer, *Inorg. Chem.* **1990**, *29*, 2370.

  

[11] a) G. van Koten, S. L. James, J. T. B. H. Jastrzebski, *Comprehensive Organometallic Chemistry II, Vol. 3* (Eds.: E. W. Abel, F. G. A. Stone, G. Wilkinson), Pergamon, Oxford, **1995**, p. 57; b) G. van Koten, J. G. Noltes, *Comprehensive Organometallic Chemistry, Vol. 3* (Eds.: G. Wilkinson, F. G. A. Stone, E. W. Able), Pergamon, Oxford, **1982**, p. 709; c) A. J. Edwards, M. A. Paver, P. R. Raithby, M. Rennie, C. A. Russell, D. S. Wright, *Organometallics* **1994**, *13*, 4967.
[12] Vibrational frequency analysis showed a very small imaginary frequency of $6i\,cm^{-1}$ for the [HOMO−2→LUMO+2] excited state. Since the imaginary value is so small, this excited state is considered as a minimum.
[13] J. Cirera, P. Alemany, S. Alvarez, *Chem. Eur. J.* **2004**, *10*, 190.
[14] R. A. Marcus, *Annu. Rev. Phys. Chem.* **1964**, *15*, 155.
[15] J. L. Marshall, S. R. Stobart, H. B. Gray, *J. Am. Chem. Soc.* **1984**, *106*, 3027.
[16] J. Hermolin, M. Levin, E. M. Kosower, *J. Am. Chem. Soc.* **1981**, *103*, 4808.
[17] a) M. E. Barr, P. H. Smith, W. E. Antholine, B. Spencer, *J. Chem. Soc. Chem. Commun.* **1993**, 1649; b) M. B. Robin, P. Day, *Adv. Inorg. Chem. Radiochem.* **1967**, *10*, 247; c) B. Scott, R. Willett, L. Porter, J. Williams, *Inorg. Chem.* **1992**, *31*, 2483; d) R. R. Gagné, C. A. Koval, T. J. Smith, *J. Am. Chem. Soc.* **1977**, *99*, 8367; e) R. R. Gagné, C. A. Koval, T. J. Smith, M. C. Cimolino, *J. Am. Chem. Soc.* **1979**, *101*, 4571.
[18] V. W.-W. Yam, K. K.-W. Lo, C.-R. Wang, K.-K. Cheung, *J. Phys. Chem. A* **1997**, *101*, 4666.
[19] T. Watanabe, K. Honda, *J. Phys. Chem.* **1982**, *86*, 2617.
[20] G. J. Kubas, *Inorg. Synth.* **1979**, *19*, 90.
[21] R. Wu, J. S. Schumm, D. L. Pearson, J. M. Tour, *J. Org. Chem.* **1996**, *61*, 6906.
[22] G. E. Coates, C. Parkin, *J. Chem. Soc.* **1962**, 3220.
[23] G. M. Sheldrick, SHELX97, Programs for Crystal Structure Analysis (Release 97–2), University of Göttingen, Germany, **1997**.
[24] M. J. Frisch, et al., *Gaussian 03*, Revision C.02, Gaussian, Inc.: Pittsburgh, PA, **2004**.
[25] a) M. Ernzerhof, G. E. Scuseria, *J. Chem. Phys.* **1999**, *110*, 5029; b) M. Ernzerhof, J. P. Perdew, K. Burke, *Int. J. Quantum Chem.* **1997**, *64*, 285.
[26] D. Andrae, U. Haeussermann, M. Dolg, H. Stoll, H. Preuss, *Theor. Chim. Acta* **1990**, *77*, 123.
[27] T. H. Dunning, Jr., P. J. Hay in *Modern Theoretical Chemistry* (Ed.: E. H. Schaefer III), Plenum, New York, **1976**, pp. 1–28.
[28] A. W. Ehlers, M. Böhme, S. Dapprich, A. Gobbi, A. Höllwarth, V. Jonas, K. F. Köhler, R. Stegmann, A. Veldkamp, G. Frenking, *Chem. Phys. Lett.* **1993**, *208*, 111.
[29] a) H. J. Hehre, R. Ditchfield, J. A. Pople, *J. Chem. Phys.* **1972**, *56*, 2257; b) P. C. Hariharan, J. A. Pople, *Theor. Chim. Acta* **1973**, *28*, 213; c) M. M. Francl, W. J. Pietro, W. J. Hehre, J. S. Binkley, M. S. Gordon, D. J. Defrees, J. A. Pople, *J. Chem. Phys.* **1982**, *77*, 3654; d) T. Clark, J. Chandrasekhar, G. W. Spitznagel, P. V. R. Schleyer, *J. Comput. Chem.* **1983**, *4*, 294.

Received: March 13, 2006
Published online: July 3, 2006

  